

1 **REVISION 1**

2 **TITLE**

3 **CRYSTAL CHEMISTRY AND LIGHT ELEMENTS ANALYSIS OF Ti-RICH GARNETS**

4
5 Schingaro Emanuela¹, Lacalamita Maria^{1*}, Mesto Ernesto¹, Ventruti Gennaro¹, Pedrazzi
6 Giuseppe², Ottolini Luisa³, Scordari Fernando¹
7

8 ¹Dipartimento di Scienze della Terra e Geoambientali, Università degli Studi di Bari “Aldo Moro”,
9 via E. Orabona 4, I-70125, Bari, Italy

10 ²Dipartimento di Neuroscienze, Università di Parma, via Volturno 39, I-43100, Parma, Italy

11 ³CNR-Istituto di Geoscienze e Georisorse, Unità di Pavia, via A. Ferrata 1, I-27100 Pavia, Italy
12
13
14
15
16
17
18
19
20
21
22
23
24
25
26

27
28
29 submitted to: *American Mineralogist*
30 address of the corresponding author:
31 Prof. Emanuela Schingaro
32 Dipartimento di Scienze della Terra e Geoambientali,
33 Università degli Studi di Bari “Aldo Moro”
34 Via Orabona 4, I-70125 Bari, Italy
35 Phone 0039-080-5443578
36 e-mail: emanuela.schingaro@uniba.it

ABSTRACT

A suite of Ti-bearing garnets from magmatic, carbonatitic and metamorphic rocks was studied by Electron Probe Microanalysis (EPMA), X-ray Powder Diffraction (XRPD), Single Crystal X-ray Diffraction (SCXRD), Mössbauer spectroscopy and Secondary Ion Mass Spectrometry (SIMS) in order to better characterize their crystal chemistry. The studied garnets show TiO_2 varying in the ranges 4.9(1) - 17.1(2) wt% and variable $\text{Fe}^{3+}/\Sigma\text{Fe}$ content. SIMS analyses allowed quantification of light elements yielding H_2O in the range 0.091(7) - 0.46(4), F in the range 0.004(1) - 0.040(4) and Li_2O in the range 0.0038(2) - 0.014(2) wt%. Mössbauer analysis provided spectra with different complexity, which could be fitted to a number of components variable from one ($^Y\text{Fe}^{3+}$) to four ($^Y\text{Fe}^{2+}$, $^Z\text{Fe}^{2+}$, $^Y\text{Fe}^{3+}$, $^Z\text{Fe}^{3+}$). A good correlation was found between the $\text{Fe}^{3+}/\Sigma\text{Fe}$ resulting from the Mössbauer analysis and that derived from the Flank method.

X-ray powder analysis revealed that the studied samples are a mixture of different garnet phases with very close cubic unit cell parameters as recently found by other authors. Single crystal X-ray refinement using anisotropic displacement parameters were performed in the $1a\bar{3}d$ space group and converged to $1.65 \leq R_1 \leq 2.09$ % and $2.35 \leq wR_2 \leq 3.02$ %. Unit cell parameters vary in the range $12.0641(1) \leq a \leq 12.1447(1)$ Å, reflecting different Ti contents and extent of substitutions at tetrahedral site.

The main substitution mechanisms affecting the studied garnets are: $^Y\text{R}^{4+} + ^Z\text{R}^{3+} \leftrightarrow ^Z\text{Si} + ^Y\text{R}^{3+}$ (schorlomite substitution); $^Y\text{R}^{2+} + ^Z\text{R}^{4+} \leftrightarrow 2^Y\text{R}^{3+}$ (morimotoite substitution); $^Y\text{R}^{3+} \leftrightarrow ^Y\text{Fe}^{3+}$ (andradite substitution); in the above substitutions $^Y\text{R}^{2+} = \text{Fe}^{2+}, \text{Mg}^{2+}, \text{Mn}^{2+}$; $^Z\text{R}^{4+} = \text{Ti}$; $^Y\text{R}^{3+} = \text{Fe}^{3+}, \text{Al}^{3+}, \text{Cr}^{3+}$; $^Z\text{R}^{3+} = \text{Fe}^{3+}, \text{Al}^{3+}$. Minor substitutions, such as $2^Y\text{Ti}^{4+} + ^Z\text{Fe}^{2+} \leftrightarrow 2^Y\text{Fe}^{3+} + ^Z\text{Si}$, $(\text{SiO}_4)^{4-} \leftrightarrow (\text{O}_4\text{H}_4)^{4-}$, $\text{F}^- \leftrightarrow \text{OH}^-$ and $^Y\text{R}^{4+} + ^X\text{R}^+ \leftrightarrow ^Y\text{R}^{3+} + ^X\text{Ca}^{2+}$, with $^Y\text{R}^{4+} = \text{Ti}, \text{Zr}$; $^Y\text{R}^{3+} = \text{Fe}^{3+}, \text{Al}, \text{Cr}^{3+}$; $^X\text{R}^+ = \text{Na}, \text{Li}$ also occur.

62
63

64 **Keywords:** Ti-bearing garnets, light elements, SCXRD, XRPD, EPMA, SIMS, Mössbauer
65 spectroscopy, crystal chemistry.

66
67
68
69
70
71
72
73
74
75
76
77
78
79
80
81
82
83
84
85
86
87
88
89
90
91
92
93

INTRODUCTION

Garnets are a supergroup of rock-forming minerals, with generalized chemical formula $\{X_3\}[Y_2](Z_3)\phi_{12}$ where dodecahedral $\{X\}$, octahedral $[Y]$ and tetrahedral (Z) are the three symmetrically unique atomic sites and the anionic site (ϕ) represents O^{2-} , OH^- , and F^- (Grew et al. 2013). Alternating $Z\phi_4$ tetrahedra and $Y\phi_6$ octahedra share corners to form a three-dimensional framework containing $X\phi_8$ triangular dodecahedra.

These minerals are widespread in the Earth's crust, upper mantle and transitional zone and occur in a variety of rocks. In a recent revision of the nomenclature of garnets (Grew et al. 2013), thirty-two species of the garnet supergroup were approved, out of which twenty-nine were further divided into five groups, on the basis of the symmetry and of the total charge of cations at the tetrahedral site: henritermierite (tetragonal, Z charge = 8), bitikleite (cubic, Z charge = 9), schorlomite (cubic, Z charge = 10), garnet (cubic, Z charge = 12), berzellite (cubic, Z charge = 15). Ti-garnets may belong to the schorlomite or to the garnet group, depending on the composition and cation distribution (see below). In previous literature, Ti-garnets are referred to as Ti-bearing andradite, melanite, schorlomite and morimotoite, and Chakhmouradian and McCammon (2005) reviewed the criteria historically used to distinguish between melanite and schorlomite. From a geological viewpoint, Ti-rich garnets are found in various silica undersaturated alkaline igneous rocks (Huggins et al. 1977a, 1977b; Dingwell and Brearley 1985; Gwalani et al. 2000; Saha et al. 2011) and are related to alkali metasomatism and magmatism of carbonatitic affinity (Platt and Mitchell 1979; Deer et al. 1982).

Depending on the species occupying the crystallographic sites, they may be used as tracers of magma evolution (Lupini et al. 1992; Gwalani et al. 2000; Brod et al. 2003), as indicators of f_{O_2} , f_{H_2O} and other thermodynamic parameters active during the mineral crystallization. In addition, their crystal chemistry is recognized to affect the partitioning of trace elements between the garnets and

the melt, and this information can be used to constrain petrogenetic processes in planetary interiors (Dwarzski et al. 2006).

However, the determination of the correct crystal chemistry of garnets is very complex because of the great number of substituting cations over the three independent crystallographic sites and, with particular regards to Ti-rich garnets, of the multiple oxidation states and coordination environments of transition elements such as Fe and Ti. This topic has been thoroughly reviewed by Grew et al. (2013), also in view of the relevant implications for classification and nomenclature of garnets.

Ti-garnets may also incorporate hydrogen, fluorine, lithium in trace but measurable amounts. In particular, the OH-bearing garnets may be a reservoir of hydrogen in the Earth's mantle and may also affect the evolution of the hydrosphere through its influence on mantle melting and isotopic fractionation (Bell et al. 2004).

Quantitative analysis of trace hydrogen is therefore necessary for a better understanding of its role in geological processes but, unfortunately, there is no routinary method to obtain this information. For instance, the hydrogen content (conventionally quantified as H₂O, wt%) in schorlomite and Ti-andradite was often estimated from the summed integrated OH⁻ absorbance in the infrared spectra using a wavenumber-dependent calibration (Lager et al. 1989; Müntener and Hermann 1994; Locock et al. 1995; Amthauer and Rossman 1998; Katerinopoulou et al. 2009; Phichaikamjornwut et al. 2011). Actually, it has been demonstrated that the choice of a calibration method for garnets is not unambiguous since considerable discrepancies exist among the available calibrations (e.g., Maldener et al. 2003). The hydrogen content of titanite andradites from Sanbagawa metamorphic rocks (Central Japan), melilitic rocks of the Osečná complex (Bohemia) and schorlomite from Afrikanda (Kola Peninsula) silicocarbonatite was measured respectively by means of wet analysis, gravimetry and combustion (Onuki et al. 1982; Ulrych et al. 1994;

Chakhmouradian and McCammon 2005). Kühberger et al. (1989) used the solid's moisture analyzer to determine the water content in synthetic Ti-andradite.

Multiple mechanisms have been proposed to describe the hydrogen uptake in garnets. The hydrogarnet substitution ($4\text{H} + {}^{\text{Z}}[\text{}] \rightarrow [\text{}] + {}^{\text{Z}}\text{Si}$), where, i.e., a SiO_4 unit may be replaced by H_4O_4 on the tetrahedral site, was often invoked because consistent with diffraction technique data from H-rich samples (e.g., Lager et al. 1987, 1989; Eeckhout et al. 2002; Ferro et al. 2003). Evidences from electron microprobe data, nuclear magnetic resonance (NMR) and infrared (IR) spectra have been reported as pointing to octahedral and dodecahedral hydrogen occupancy in garnets (Basso et al. 1984a, b; Kalinichenko et al. 1987; Basso and Cabella 1990; Rossman and Aines 1991).

Fluorine content of Ti-andradites or titanium andradites-grossular was mainly obtained by electron-microprobe analysis (Flohr and Ross 1989; Manning and Bird 1990; Barbanson and Bastos Neto 1992; Visser 1993; Ulrych et al. 1994; Freiburger et al. 2001; Faryad and Dianiška 2003) but also by F-sensitive glass electrode (Armbruster et al. 1998). Exchange reaction $\text{F}^- \leftrightarrow \text{OH}^-$ was used to explain the incorporation of fluorine in garnet, but also more complex reactions were proposed involving coupled cations substitutions for charge balance (Valley et al. 1983).

To the best of our knowledge, studies on lithium in Ti-garnets, instead, are missing in literature. For natural or synthetic Ti-free, Li-rich garnets it was proposed that lithium occupies not only the Z but also the Y, X and interstitial 96h sites (Cussen 2006; Cempírek et al. 2010). These garnets have high-ionic conductivity (e.g. Wang and Lai 2012) or notable implications as a geobarometer (Yang et al. 2009).

In the present study, hydrogen, fluorine and lithium were measured in a suite of Ti-garnets from a variety of rock types by means of secondary ion mass spectrometry (SIMS). This technique was only previously used to derive an H_2O calibration curve employing, however, garnets with pyralspite composition, whose hydrogen abundance were determined by manometry and IR measurements (Koga et al. 2003).

The results of SIMS, electron microprobe analysis (EPMA), X-ray powder diffraction (XRPD), single crystal X-ray diffraction (SCXRD) and Mössbauer spectroscopy have been here integrated in the present study of Ti garnets of different origin and provenance in order to provide a comprehensive crystal chemical characterization of the studied samples.

MATERIALS AND METHODS

Samples

The analysed samples are from different geologic environments: magmatic alkaline, carbonatitic and metamorphic rocks. The details of samples origin and provenance are reported in **Table 1**. Most of the analysed samples have been previously partially characterized and the relevant results published in the papers reported in the last column of **Table 1**. In the present work, for the first time a full crystal chemical characterization is accomplished for W6 and W16 samples. In addition, a re-examination of the crystal chemical formulae of W12, NZALA and ZER2 samples, previously studied by some of the authors, is here proposed on the basis of EPMA, SIMS, XRPD and SCXRD measurements on new crystals. Non routinary chemical analysis (EPMA with the Flank method, SIMS see below) are reported for the first time on the whole suite of study samples as well as the results of XRPD measurements.

EPMA

Quantitative elemental analyses of the studied crystals (embedded in epoxy resin and polished) were performed with a JEOL JXA-8200 electron microprobe (Dipartimento di Scienze della Terra, University of Milano) operating at 15 kV acceleration voltage, 5 nA beam current, ~ 1 µm beam size and 30s counting time. All the elements were analysed in wavelength dispersive spectrometry (WDS) mode and the adopted standards were: wollastonite (Si), anorthite (Al, Ca), olivine (Mg), fayalite (Fe), omphacite (Na), ilmenite (Ti), Cr pure (Cr), rhodonite (Mn) and zircon

jarosite (Zr). A Phi-Rho-Z routine as implemented in the JEOL suite of programs was used for the matrix correction. Analytical measurements were affected by a relative uncertainty of 1% for major elements and 4% for minor elements. 'Flank method' measurements for the determination of the $\text{Fe}^{3+}/\Sigma\text{Fe}$ were carried out with the same electron microprobe as above, in WDS mode, employing a TAP crystal and a 300 μm slit. $\text{FeL}\beta$ and $\text{FeL}\alpha$ peaks were searched and measured for counting times of 300 s. The correction for self-absorption was applied (Höfer and Brey 2007) and natural and synthetic garnet end-members with fixed $\text{Fe}^{3+}/\Sigma\text{Fe}$ were used as standards (Malaspina et al. 2009). The accuracy of the Flank method has been defined by a maximum error of ± 0.04 for $\text{Fe}^{3+}/\Sigma\text{Fe}$ in samples with total Fe in the range 8-11 wt % (Höfer and Brey 2007).

SIMS

SIMS analyses were performed with the ion microprobe Cameca IMS 4f installed at CNR-IGG (Pavia) following procedures similar to those reported in Ottolini et al. (1995, 2002). A static, mass filtered $^{16}\text{O}^-$ primary beam accelerated to 12.5 kV was focused on the sample surface to obtain a current intensity of 9.5 nA, corresponding to $\sim 15 \mu\text{m}$ beam diameter. The second aperture (400 μm \varnothing) on the primary-beam selector was used to prevent $^{16}\text{O}^1\text{H}^-$ ions, which forms a weak second spot on the sample (clearly visible in anhydrous samples), from reaching the ion probe sample chamber (SC). Positive secondary ions from the sample were extracted by a 4.5 kV accelerating voltage and transferred into the mass spectrometer by the 25 μm secondary-ion optics. Secondary ions were "energy filtered" with an emission energy in the range ~ 75 -125 eV. H^+ , $^7\text{Li}^+$, $^{19}\text{F}^+$ and $^{30}\text{Si}^+$ ion signals were detected after 450-sec waiting time required to get steady-state sputtering conditions. Acquisition times were 3s for H^+ and $^7\text{Li}^+$ each, 8s for $^{19}\text{F}^+$ and 3s for $^{30}\text{Si}^+$ for each of the two analytical cycles. Hydrogarnet crystals and standards were left to degas seven days in the ion probe SC before running analysis. Detection limits for H (6σ background) were estimated on the order of 20 ppm H.

The results for H, Li and F were put on a quantitative basis using empirical calibration curves based on standards that were the following: schorl (no. 16), dravite (no. 18), elbaite (no. 19), fully characterized in Ottolini et al. (2002). In particular, for H quantification we used the extrapolated regression line: $IY(H/Si)$ vs. $(Fe_{tot}+Ti+Mn)(at)$, first derived in kornerupine (Ottolini and Hawthorne 2001) and then successfully tested in several silicate matrixes (see for instance, Scordari et al. 2010 and reference therein). The analytical accuracy for Li is on the order of 5% relative. An accuracy of better than 10% relative is quoted for H and F.

Mössbauer spectroscopy

Mössbauer spectra were recorded on powdered samples (~ 10 mg) at room temperature, in transmission geometry, using a source of $^{57}Co/Rh$ matrix (~ 1GBq) and a constant acceleration spectrometer. Spectra were recorded using a multichannel analyzer (1024 or 512 channels) in the velocity range ± 4 mm/s and subsequently folded (Shenoy et al. 1978). More than 10×10^6 baseline counts per channel were recorded for each spectrum. Isomer shifts (IS) are expressed relative to α -iron. The spectra were fitted with routines employing Levenberg-Marquardt methods and implemented in the software RECOIL 1.03a (Lagarec and Rancourt 1997, 1998).

XRPD

X-ray powder diffraction patterns were recorded using a Panalytical Empyrean diffractometer equipped with a PIXcel-3D detector. $Cu K\alpha$ radiation ($\lambda = 1.5418 \text{ \AA}$) was employed and the instrument operated at 40 kV/40 mA. Because of the shortage of samples, powders were loaded in a zero background silicon sample holder and slightly compressed with a glass slide. The patterns were collected in the 2θ range of 5° - 140° . The divergence and antiscatter slits were $1/8$ and $1/4$ mm, respectively, and the detector slit was 7.5 mm. Qualitative phase analysis was performed by means of the PANalytical HighScore software. Quantitative analysis and the refinement of the

lattice parameters were carried out by the Rietveld Method (Young 1993) as implemented in the GSASII software (Toby and Von Dreele 2013).

SCXRD

Single crystal X-ray diffraction data were collected using a Bruker AXS X8 APEXII automated diffractometer (Dipartimento di Scienze della Terra e Geoambientali, University of Bari) with a charge coupled device (CCD) detector and a four-circle Kappa goniometer. The X-ray data were acquired using a graphite monochromatized MoK α radiation, several ω and ϕ rotation scans, 1.0° scan width, 10 s per frame exposure time, crystal-to-detector distance of 40 mm and operating conditions of 50 kV and 30 mA. The COSMO program of the Apex program suite (Bruker 2003a) was used to optimize the data collection strategy whereas for cell determination and data reduction the SAINT (Bruker 2003b) and SADABS programs (Sheldrick 2003) were employed. Least-squares refinements were performed using the program CRYSTALS (Betteridge et al. 2003) in the space group $Ia\bar{3}d$. Scale factor, atomic positions, cation occupancies and anisotropic displacement factors were refined. Fully ionized scattering factors were used. Since compositional disorder can affect all three independent sites in the garnet structure (see the **Introduction** section) different cation distribution were tested in order to obtain the best fit between mean atomic numbers estimated via EPMA and structure refinement (X-ref). Preliminary refinements allowed to ascertain that tetrahedral site occupancy could assume values less than 1, indicating the occurrence of tetrahedral vacancies. In addition, the refined tetrahedral mean atomic number could be less or greater than 14e⁻, indicating respectively the presence of a lighter or a heavier substituent of Si atoms. Also Ca occupancy was initially left free to vary to check for the occurrence of Fe²⁺ at X (in this case the mean atomic number would refine to more than 20 e⁻). In final refinements, depending of the bulk chemistry of each sample, the following refinement restrictions (Watkin 2008) were used:

- 1) at the X-site, the occupancies of Ca, or Ca and Mg (the latter representing also Na atoms) were restrained so that the site was fully occupied;
- 2) at the Y-site, the Al and Fe occupancies (with Fe representing Mn + Ti (+ Zr) and Al representing Mg scattering species) were restrained to obtain a full occupancy;
- 3) at the Z-site, the Si (standing also for Al), or Si and Fe occupancies were refined with a restraint which could result in a total occupancy less, equal or greater than 1.

RESULTS AND DISCUSSION

Chemical composition

EPMA data calculated as average over 4-10 spots are reported in **Table 2** together with SIMS data. Indeed, the within grain coefficient of variation (CV) is < 10% for all the measured oxides with the exception of Na₂O, ZrO₂, Cr₂O₃, whereas as far as light elements are concerned, it is ~ 10% for H₂O, generally > 50% for Li₂O and variable (4-44%) for the F content.

In particular, the studied Ti-garnets are characterized by variable degree of hydration. SIMS analyses provide H₂O concentration in the range 0.091(7)-0.46(4) wt% (**Table 2**) which is in agreement (see also **Figure 1**) with the values measured for most of the Ti-garnets with andradite, andradite-grossular, andradite-uvarovite or schorlomite component (Müntener and Hermann 1994; Locock et al. 1995; Amthauer and Rossman 1998; Chakhmouradian and McCammon 2005; Katerinopoulou et al. 2009; Phichaikamjornwut et al. 2011). However, higher H₂O contents (from 1.25 to 2.90 wt%) were reported for other Ti-garnets (Onuki et al. 1982; Lager et al. 1989; Ulrych et al. 1994; Amthauer and Rossman 1998). Galuskin (2005) calculated, on the basis of charge balance, ~ 5 wt% H₂O in the “hydroschorlomite” whereas up to 10 wt% H₂O was estimated from cell dimensions considerations in the “hydroandradite” (Armbruster 1995).

Very low amount of Li₂O (0.0038(2) - 0.014(2) wt%) equivalent to 0.001-0.005 atoms per formula unit was detected in the studied samples (**Table 2**). These values are similar to those (0-

0.004 apfu) found in Ti-free garnets (Grew et al. 1990). Cempírek et al. (2010) measured 0.019-0.079 Li pfu in almandine from leucocratic granulite of Czech Republic. For synthetic Li-rich majoritic garnet, Yang et al. (2009) provide 1.96 Li pfu whereas up to about 7 Li atoms pfu were reported for other synthetic garnets (Wang and Lai 2012). This element occurs as a major chemical component in the garnet end member cryolithionite, $\text{Na}_3\text{Al}_2\text{Li}_3\text{F}_{12}$ (Geller 1971).

Regarding the fluorine concentration, in our samples it ranges from 0.004(1) to 0.040(4) wt% (**Table 2**) which corresponds to 0.001-0.010 atoms per formula unit. Literature data indicate F content ranging from ~ 0.1 to 5 wt% in Ti-garnets with andradite and andradite-grossular component (Flohr and Ross 1989; Manning and Bird 1990; Barbanson and Bastos Neto 1992; Visser 1993; Ulrych et al. 1994; Armbruster et al. 1998; Freiburger et al. 2001; Faryad and Dianiška 2003) and is equal to ~ 6 wt% in the F-rich hibschite (Chakhmouradian et al. 2008), showing that in our garnets all values are on the lower end of the natural variability interval.

Iron speciation

The iron oxidation state was determined both via electron microprobe analysis – the Flank method (Höfer and Brey 2007) - and Mössbauer spectroscopy. Specifically, the Flank method was used on the same single crystals which underwent structure refinements, whereas Mössbauer analyses were carried out on powders of the W6 and W16 samples. The results are reported respectively in **Tables 2** and **3**. Mössbauer spectra of samples W6 and W16 are in **Figure 2a, 2b**, whereas comparison between Mössbauer and Flank method is in **Figure 3**. In **Table 3** Mössbauer data on W12, NZALA and ZER2 samples from previous work (Pedrazzi et al. 2002) are also reported for comparison. The fitting of the room temperature Mössbauer spectra **Figure 2** allowed to identify different iron species: $^{\text{Y}}\text{Fe}^{3+}$, $^{\text{Z}}\text{Fe}^{3+}$, $^{\text{Z}}\text{Fe}^{2+}$, $^{\text{Y}}\text{Fe}^{2+}$. The assignment and the values of the hyperfine parameters (**Table 3**) are in agreement with the results of previous investigations on Ti-garnets (Ortalli et al. 1994; Pedrazzi et al. 1998, 2002; Scordari et al. 1999; Schingaro et al. 2004;

Dyar et al. 2012). In particular, the $^Z\text{Fe}^{2+}$ species has been reported in other Mössbauer spectra on Ti-garnets (Kühberger et al. 1989; Locock et al. 1995; Chakhmouradian and McCammon 2005) but its interpretation is still uncertain and, recently, Chakhmouradian and McCammon (2005) have reinterpreted this component as $^Y\text{Fe}^{2+} \leftrightarrow ^Z\text{Fe}^{3+}$ electron transfer. However, attempts to fit the spectra of W6, W16 and NZALA samples according to the model 2 in Chakhmouradian and McCammon (2005) were unsuccessful.

The comparison between $\text{Fe}^{3+}/\Sigma\text{Fe}$ as measured by Mössbauer and Flank method derived (**Figure 3**) indicates a good correlation ($R^2 \sim 0.8$) between the two sets of measurements. The observed discrepancies, specifically for the W12 and W16 samples, may be due to the crystal chemical heterogeneity of the sample, so that the single crystals selected for EPMA and SCXRD may be not representative of the powders (see also the section XRPD below).

Structural features

XRPD results

The X-ray powder diffraction analysis was performed on all the study samples (see the patterns in **Figure 4**) with the exception of ZER2, whose amount was too scarce to be measured. The qualitative analysis evidenced that no phase impurity occurs. However, splitting or asymmetry of the diffraction peaks is observed, suggesting the presence in our powders of different garnet phases with similar unit cell parameters (**Figure 5**). Indeed in all samples, at least two cubic garnet phases (labelled phase I and II on the basis of the relative abundances) were clearly distinguished and their weight fractions and cell parameters were refined using GSASII; the results are shown in **Table 4**. In the case of W6 and W16 samples, a third phase seems to be present (**Figure 5**) but the attempts to refine it was unsuccessful. These results are in agreement with recent findings relevant to the study of optical anomalies in garnets. In particular, these studies have shown that both Ti-bearing and Ti-free garnets can actually be a mixture of two or more cubic phases with slightly

different cell parameters and composition (Antao 2013, 2014; Antao and Klincker 2013; Antao and Round 2014). The consequent structural mismatch causes strain that results in low- to -strong degree of optical anisotropy (birefringence). In our case, the garnets appear not completely extinct upon observation under cross-polarized light, but did not show difference in chemical composition at least at the EPMA scale (see above). Similar results were reported for a Ti-andradite from Magnet Cove (Antao 2013). In brief, anomalous optical behavior is due to intergrowth of more than one cubic phase, that, if occurs at a fine scale, leads to homogeneous EPMA data, whereas at a large scale should be detected as a slight variation of chemical composition. To the best of our knowledge, it is the first time that a mixture of cubic phases has been detected for Ti-garnets with laboratory instrumentation. In addition, data in **Table 4** show that the dominant phase of the mixture (phase I) has, in most cases, unit cell parameters similar to those obtained from the relevant samples in SCXRD analysis (see below).

SCXRD results

The main results of SCXRD investigation, in particular about crystal data, data-collection parameters and figures of merit on structure refinements, are also summarised in **Table 4**. Refined site positions, atomic occupancies and anisotropic displacement parameters are listed in **Table 5** whereas distances and distortional parameters are reported in **Table 6**.

All structure refinements converged to good values of the discrepancy factors: $1.65 \leq R_1 \leq 2.09 \%$ and $2.35 \leq wR_2 \leq 3.02 \%$.

The cell-edges variation of the analysed crystals (**Table 4**) reflects different Ti contents (**Table 2**), a correlation already pointed out by Howie and Woolley (1968). In particular, a positive trend of the a parameter versus the TiO_2 content has been found (**Figure 6**).

However, by inspection of **Figure 7** it is evident that the a -cell parameter increment depends on the increase of both the $\langle\text{X-O}\rangle$ ($R^2 = 0.90$ in **Figure 7a**) and Z-O ($R^2 = 0.86$ in **Figure 7c**)

whereas the dependence from the Y-O variation seems to be negligible ($R^2 = 0.004$ in **Figure 7b**). Since the X-site composition is almost constant in the study samples (see **Table 7**), the increase of $\langle X-O \rangle$ is induced by the polyhedral edge-sharing (X/Z) occurring in the garnet structure.

From **Table 6** it can be noticed that the $\Delta(X-O)$ and α values are in the range of variability for the known natural silicate garnets (Ungaretti et al. 1995; Yang et al. 2009). The tendency to the decrease of $\Delta(X-O)$ with increasing Fe^{3+} content along the grossular-andradite join (Ungaretti et al. 1995) is also present in our samples, where it appears also related to the $Fe^{3+} + Ti$ content.

Octahedral and tetrahedral sites in garnets are variously distorted, as evident from the analysis of octahedral angle variance and tetrahedral angle variance (OAV and TAV, **Table 6**) which, respectively, quantifies the deviation from the ideal value of 90° and 109.47° of the relevant polyhedra (**Table 6**, **Figures 8** and **9**). In particular, the tetrahedron is the most distorted polyhedron in garnets and the distortion increases with increasing the $Z(Fe^{2+}+Al+Fe^{3+}+Ti)$ content (**Figure 8**). On the other hand, since each tetrahedron in the garnet structure shares edges with two dodecahedra, the shared O-O tetrahedral edges, $S(Z)$, are always shorter than the unshared ones, $U(Z)$ and, at the same time, the tetrahedron is elongated along the $\bar{4}$ axis (see t_{SZ} , the distance between shared edges in **Table 6**) for a better screening of the repulsive interaction between the X and Z cations. The octahedron is most distorted in grossular and becomes more regular with the entrance of high charge cations or of trivalent cations different from Al^{3+} (**Figure 9**). In addition, substitutions at Y affect the t_{SY} parameter in that, starting from pure grossular, where the octahedron is flattened along the $\bar{3}$ axis, if a cation larger than Al occurs at Y the octahedron tends to elongate along the same axis, as also observed by other authors (Ungaretti et al. 1995).

The ZER2 sample has bond distances and distortion parameters very similar to that of pure andradite (Adamo et al. 2011). For instance, for this sample the $\langle D-O \rangle$ parameter (2.131 Å) is identical to that of the pure andradite (2.132 Å, Adamo et al. 2011) and is a consequence of its short

Z-O distance (**Table 6**), indicating a low extent of substitution at the Z site. The increase in the Z-O distances in the other samples accounts for a greater extent of schorlomitic and hydrogarnet substitutions. These features entail the increase of the $\langle D-O \rangle$ parameters up to values close to that (2.186 Å) of kimzeyite of Schingaro et al. (2001), see **Table 6**.

Crystal chemical formulae

Grew et al. (2013) suggested a procedure to perform a cation distribution for Ti-garnets basing only on chemical data; the results obtained using their spreadsheet are reported in **Table 7**. In the same table we also reported the structural formulae of the study garnets, obtained using a multimethodic approach adopted in the present work. Specifically, they were calculated combining the EPMA-SIMS data with the Mössbauer results. The latter were considered representative of the single crystals. This assumption is generally sensible, on the basis of the Flank method analysis (see above). From the two sets of crystal chemical formulae, mean atomic numbers as well as bond distances using ionic radii from Shannon (1976) have been calculated. These values are shown in **Table 8** where they are compared with those derived from the structure refinement.

Samples W12 and ZER2 contain the smallest number of Fe species ($^Y\text{Fe}^{3+}$, $^Z\text{Fe}^{3+}$ the former and only $^Y\text{Fe}^{3+}$ the latter, see **Table 3**) and in particular ZER2 has the simplest composition among the whole suite here considered. Comparison to the formulae derived through the approach devised by Grew et al. (2013) indicates that charge balance tends to overestimate the $^Y\text{Fe}^{2+}$ specie. For example, for the ZER2 garnet, both the Flank method and Mössbauer analysis provide $\text{Fe}^{3+}/\Sigma\text{Fe} = 100\%$, whereas from Grew et al. (2013) $\text{Fe}^{3+}/\Sigma\text{Fe} = 86\%$ is estimated (see **Tables 2, 3, 7** and **Figure 3**). Comparison to the crystallographic data (**Table 8**) shows that a better agreement is obtained with our multi-methodic approach for the Y site, that allows a better modeling of this site in terms of mean atomic number as well as bond distances. In particular good agreement is found between the Y-O distance derived from the X-ray refinement ($\text{Y-O}_{\text{X-ref}}$) and that calculated from the EPMA

(Y-O_{EPMA*}) with $\Delta = (\text{Y-O}_{\text{X-ref}}) - (\text{Y-O}_{\text{EPMA*}}) = 0.008 \text{ \AA}$ (see **Table 8**). On the contrary, if the approach in Grew et al. (2013) is used, Δ increases to 0.021 \AA . Note that the use of the directly measured iron speciation implies that the Y site hosts significant amount of Ti³⁺, as previously found in the Val Malenco Ti-bearing garnets (Müntener and Hermann, 1994; 175, 274, 275, 276 crystals in Merli et al. 1995). As found for the sample ZER2, also in sample W12 ^YFe²⁺ is overestimated, since Mössbauer spectrum only shows Fe³⁺ species (**Tables 2, 3**) and our formula, as before, provides a better modeling of the octahedral site.

In the case of sample W6 the Mössbauer spectrum is more complex and in particular the ^ZFe²⁺ species has been detected. Although controversial (Chakhmouradian and McCammon 2005) this species is taken into account by Grew et al. (2013) in the procedure for site allocation of cations in Ti-garnets. However, the substitution explaining the ^ZFe²⁺ uptake in the garnet structure is not specified. In the literature two mechanisms have been proposed for the charge balance in this case: ^ZSi⁴⁺ + 2O²⁻ ↔ ^ZR²⁺ + 2(OH)⁻ (Kühberger et al. 1989) and 2^YTi⁴⁺ + ^ZFe²⁺ ↔ 2^YFe³⁺ + ^ZSi (Locock et al. 1995). Another mechanism ^YU⁶⁺ + ^ZFe²⁺ = ^YU⁵⁺ + ^ZFe³⁺ was proposed for elbrusite (Galuskina et al. 2010a). In our case, the mechanism of Kühberger et al. (1989) leads to major inconsistencies with SIMS data relevant to the hydrogen quantification. Accordingly, the mechanism proposed by Locock et al. (1995) was adopted.

For sample NZALA, that contains negligible ^ZFe²⁺, our distribution and the one from Grew et al. (2013) are almost identical. Notice that the calculated and measured Fe³⁺/ΣFe values are very similar (see **Tables 2, 3**). Although a general good agreement with X-ray data is observed for both formulae, the difference between Y-O_{EPMA} and Y-O_{X-ref} distances gives < 0.01 \AA in our case and ~ 0.02 \AA considering only chemical data (see **Table 8**).

For sample W16, Mössbauer and charge balance derived Fe³⁺/ΣFe coincide, whereas a discrepancy is observed with respect to the value determined via the Flank method (see **Tables 2, 3** and **Figure 3**). The difference between cell parameter from single crystal and powder is $\Delta a \sim 0.01$ -

0.02 Å. The above evidences indicate that the single crystal is not representative of the powder. Several cation distributions have been checked, until the best fit to the data from different techniques was obtained by considering $\text{Fe}^{3+}/\Sigma\text{Fe}$ from Flank method and the iron site population from Mössbauer.

Sample W6 has ferrous iron only at tetrahedral site. As in previous sample, inspection of **Table 4** evidences that the single crystal has cell parameter shorter than those found in the powder ($\Delta a \sim 0.01\text{-}0.02$ Å). Accordingly, for the study single crystal a lower degree of tetrahedral substitution is expected with respect to the analysed powder. The best fit to all the experimental data is obtained varying the $^{\text{Z}}\text{Fe}^{2+}$ component within one standard deviation.

The main substitution mechanisms affecting the studied garnets are:

- 1) $^{\text{VI}}\text{R}^{4+} + ^{\text{IV}}\text{R}^{3+} \leftrightarrow ^{\text{IV}}\text{Si} + ^{\text{VI}}\text{R}^{3+}$ (schorlomite substitution);
- 2) $^{\text{Y}}\text{R}^{2+} + ^{\text{Z}}\text{R}^{4+} \leftrightarrow 2^{\text{Y}}\text{R}^{3+}$ (morimotoite substitution);
- 3) $^{\text{Y}}\text{R}^{3+} \leftrightarrow ^{\text{Y}}\text{Fe}^{3+}$ (andradite substitution);

where $^{\text{Y}}\text{R}^{2+} = \text{Fe}^{2+}, \text{Mg}^{2+}, \text{Mn}^{2+}$; $^{\text{Z}}\text{R}^{4+} = \text{Ti}$; $^{\text{Y}}\text{R}^{3+} = \text{Fe}^{3+}, \text{Al}^{3+}, \text{Cr}^{3+}$; $^{\text{Z}}\text{R}^{3+} = \text{Fe}^{3+}, \text{Al}^{3+}$.

Minor substitutions, such as:

- a) $2^{\text{Y}}\text{Ti}^{4+} + ^{\text{Z}}\text{Fe}^{2+} \leftrightarrow 2^{\text{Y}}\text{Fe}^{3+} + ^{\text{Z}}\text{Si}$;
- b) $(\text{SiO}_4)^{4-} \leftrightarrow (\text{O}_4\text{H}_4)^{4-}$;
- c) $\text{F}^- \leftrightarrow \text{OH}^-$;
- d) $^{\text{Y}}\text{R}^{4+} + ^{\text{X}}\text{R}^+ \leftrightarrow ^{\text{Y}}\text{R}^{3+} + ^{\text{X}}\text{Ca}^{2+}$, with $^{\text{Y}}\text{R}^{4+} = \text{Ti}, \text{Zr}$; $^{\text{Y}}\text{R}^{3+} = \text{Fe}^{3+}, \text{Al}, \text{Cr}^{3+}$; $^{\text{X}}\text{R}^+ = \text{Na}, \text{Li}$ also occur.

On the whole, light elements, although occurring in detectable amounts, do not play a significant crystal chemical role. No systematic trend was here evidenced from the analysis of Ti and water content in relation to the garnets host rocks (see also **Figure 1**).

For a better crystal chemical comparison, in **Table 7**, in addition to the structural formulae derived for the samples under study, also formulae taken from the literature are reported, selected in order to include natural end-member garnets (grossular, Novak and Gibbs 1971; andradite, Adamo

et al. 2011) as well as Z-substituted Ti garnets for which cation partition was provided on the basis of evidences from multiple methods-combination of chemical and/or X-ray diffraction and/or spectroscopic data (Müntener and Hermann 1994; Ulrych et al. 1994; Locock et al. 1995; Scordari et al. 1999; Schingaro et al. 2001; Chakhmouradian and McCammon 2005; Katerinopoulou et al. 2009; Antao 2013, 2014). It can be seen that the chemical complexity of Ti-garnets is such that every sample has to be considered on a one to one basis. In some cases, in order to get the best agreement, with X-ray data, Ti has to be distributed over octahedral and tetrahedral site (sample W6 and W16, this work; Scordari et al. 1999; Katerinopoulou et al. 2009). Evidences of the occurrence of Ti at Z site have been reported by Malitesta et al. (1995) and Armbruster et al. (1998) for garnets with similar composition, as well as in Si-poor natural garnets, like elbrusite and bitikleite (Galuskina et al. 2010a, 2010b). The Ti valence state is a controversial topic in the Ti-garnets literature and has been thoroughly reviewed by Grew et al. (2013). In particular, in natural Ti-garnets, Malitesta et al. (1995) found significant Ti^{3+} using X-ray Photoelectron Spectroscopy (XPS), whereas Waychunas (1987) and Locock et al. (1995) detected low or negligible Ti^{3+} via X-ray Absorption Near Edge Structure (XANES) spectroscopy. This discrepancy may be due to a greater contribution of the mineral surface in the case of XPS (Grew et al. 2013) as well as to the problems in the interpretation of XPS signals related to the adopted method of background removing (Guascito et al. 2014). In the present work, the Ti speciation has not been determined by direct measurements, but it was constrained indirectly through the quantification of the water content, the determination of the iron oxidation state and the balance of the substitution mechanisms in garnets.

The two approaches discussed above and used to calculate the crystal chemical formulae lead to a different classification of the study samples as shown in the plot of **Figure 10**. In particular, when the only chemical data are used, the samples fall in the schorlomite field together with the Afrikanda schorlomite (Chakhmouradian and McCammon 2005) and the morimotoite

(Antao 2014). On the contrary, when the multimethodic approach is used, the study garnets plot in the andradite field very close to most of the considered literature garnets (Müntener and Hermann 1994; Ulrych et al. 1994; Locock et al. 1995; Amthauer and Rossman 1998; Katerinopoulou et al. 2009; Phichaikamjornwut et al. 2011; Antao 2013). Notice that kimzeyite sample investigated by Schingaro et al. (2001) should be classified as belonging to the garnet group rather than to schorlomite group. Generally speaking, the approach to the garnet crystal chemical formula proposed by Grew et al. (2013) is effective and constitutes a good starting point in absence of other information, but then the obtained formula needs to be refined by comparison at least to X-ray data and possibly also to element specific techniques selected depending on the peculiar composition of the sample. Major chemical variability is, indeed, observed for the Y site, that is why a totally chemical approach is here found to have problems with the modeling cation distribution at the Y site.

IMPLICATIONS

Garnet is a widespread mineral stable in wide range of temperature (from < 300 to 2000°C) and pressure (from ambient pressure to 25 GPa). The renewed interest in the garnet species is testified by a recent issue of *Elements* (Volume 9(6), December 2013) devoted to the garnet supergroup of minerals. The relevance of elemental substitutions in determining the properties of garnets has been highlighted in Grew et al. (2013), Geiger (2013) and Antao (2013). In particular, Grew et al. (2013) evidence that recently (2009-2010) 10 new garnet species with unusual constituents were approved by the Commission on New Minerals, Nomenclature and Classification of the International Mineralogical Association and the 32 approved species also encompass three ungrouped species but new species are expected due to the extreme compositional variations in natural garnets. Geiger (2013), other than reviewing synthetic non silicate garnets and the relevant technological employment, stresses the significance of studying substitutional solid solutions in

natural garnets. Cation substitutions involve strain fields resulting in structural heterogeneities from the scale of the unit cell to the nanoscale. Structural and chemical bonding properties of garnets are believed to control element partitioning (Wood et al. 2013) and thermodynamic behavior of the garnet solid solutions. For a complete characterization of these phases, both techniques sensitive to long-range ordering (such as X-ray diffraction) and to short range ordering (spectroscopic techniques) are needed. This is the approach adopted in the present work. Regarding natural Ti-garnets, their relevance from a petrological point of view has been mentioned in the introduction section. However, it is generally recognized that determination of cation site population is really complicated for such compositions. In turn cation exchange mechanisms produce polyhedral distortions, that have been reported here, but unravelling the contribution of each of the multiple substitutions requires further work. In this study, the detailed characterization of substitution mechanisms by single crystal X-ray diffraction is associated to the observation of occurrence of multiple cubic phases from laboratory XRPD data. Even if, in our case, the samples appeared homogeneous at the EPMA scale it is here suggested that compositional differences at the nanoscale may occur, as found by other authors (Antao 2013). These findings, in turn, may have implication for the study of garnets zonation (see, for instance, Matthews et al. 1992; Gwalani et al. 2000; Agrosi et al., 2002, 2011). Complex zoning occurring in primary Ti-garnets and involving variation of Ca, Ti, Zr and Al was described by Gwalani et al. (2000). These authors were able to correlate it to the multiple events that occurred during the magma crystallization, depicting a multi-step magmatic history from fractional crystallization, to magma mixing to closed system crystallization, to fluctuation of P-T, f_{O_2} conditions. Agrosi et al. (2002) studied the sector zoning in Ti-andradite from Colli Albani and found that morimotoite substitution was present in {110} sectors whereas both morimotoite and schorlomite substitutions affected {121} sectors. The strain associated to the presence of the schorlomite substitution in {121} sectors could be correlated to the higher growth rate of these sectors with respect to the others by the layer-by layer mechanism. Subsequently, for

the same Ti-garnets from Colli Albani concentric zoning was also observed, that, together with the identification of growth marks, allowed to characterize the growth environment (Agrosi et al. 2011). Very recently (Antao et al. 2015) correlated the occurrence of multiple cubic phases in Ti-rich andradite to optical anomalies (birefringence) and to oscillatory zoning related to andradite-rich and andradite poor cubic phases or to subtle chemical variations involving Ti, Fe, Al and Mg atoms concentrations. All the above considerations indicate the high sensitivity of the Ti-garnet structure in that even slight element abundance variation has detectable effect on the crystal structure (in terms of cell edges, bond distances, etc.) as well as the potential use of the garnet crystal chemistry at the micrometric or even nanometric scale to derive geological inferences (i.e. magma evolution, thermal history, growth environment, late stage reactions, etc.).

ACKNOWLEDGMENTS

The authors are grateful to Prof. Stefano Poli (University of Milano) for the facilities at the Electron Microprobe Laboratory and Dr. Nadia Malaspina for the assistance during the ‘Flank method’ analyses at the Dipartimento di Scienze della Terra, University of Milano. Prof. Thomas Armbruster is gratefully thanked for providing NZALA and ZER2 garnet samples. Thanks are due to the Associate Editor, Gatta Giacomo Diego, and to Redhammer Günther Josef and an anonymous Referee that contributed to significantly improve the manuscript.

The XRPD laboratory at the Dipartimento di Scienze della Terra and Geoambientali, University of Bari “Aldo Moro”, was funded by Potenziamento Strutturale PONA3_00369 “Laboratorio per lo Sviluppo Integrato delle Scienze e delle Tecnologie dei Materiali Avanzati e per dispositivi innovativi (SISTEMA)”.

This work was also supported by the COFIN-MIUR.

REFERENCES

566 Adamo, I., Gatta, G.D., Rotiroti, N., Diella, V., and Pavese, A. (2011) Green andradite stones:
 567 gemmological and mineralogical characterisation. *European Journal of Mineralogy*, 23, 91-100.

568 Agrosi, G., Schingaro, E., Pedrazzi, G., Scandale, E., and Scordari, F. (2002) A crystal chemical
 569 insight into sector zoning of a titanian andradite ('melanite') crystal. *European Journal of*
 570 *Mineralogy*, 14(1), 785-794.

571 Agrosi, G., Scandale, E., and Tempesta, G. (2011) Growth marks of titanian-andradite crystals from
 572 Colli Albani (Italy). *Periodico di Mineralogia*, 80(1), 89-104.

573 Anthauer, G. and Rossman, G.R. (1998) The hydrous component in andradite garnet. *American*
 574 *Mineralogist*, 83, 835-840.

575 Antao, S.M. (2013) The mystery of birefringent garnet: is the symmetry lower than cubic?. *Powder*
 576 *diffraction*, 28(4), 281-288.

577 Antao, S.M. (2014) Crystal structure of morimotoite from Ice River, Canada. *Powder diffraction*,
 578 29(4), 325-330.

579 Antao, S.M. and Klincker, A.M. (2013) Origin of birefringence in andradite from Arizona,
 580 Madagascar, and Iran. *Physics and Chemistry of Minerals*, 40, 575-586.

581 Antao, S.M. and Round, S.A. (2014) Crystal chemistry of birefringent spessartine. *Powder*
 582 *diffraction*, 29(3), 233-240.

583 Antao, S.M., Mohib, S., Zaman, M., and Marr, R.A. (2015) Ti-rich andradites: chemistry, structure,
 584 multi-phases, optical anisotropy, and oscillatory zoning. *Canadian Mineralogist*, DOI:
 585 10.3749/canmin.1400042.

586 Armbruster, T. (1995) Structure refinement of hydrous andradite, $\text{Ca}_3\text{Fe}_{1.54}\text{Mn}_{0.20}$
 587 $\text{Al}_{0.26}(\text{SiO}_4)_{1.65}(\text{O}_4\text{H}_4)_{1.35}$, from the Wessels mine, Kalahari manganese field, South Africa.
 588 *European Journal of Mineralogy*, 7, 1221-1225.

589 Armbruster, T., Birrer, J., Libowitzky, E., and Beran, A. (1998) Crystal chemistry of Ti-bearing
 590 andradites. *European Journal of Mineralogy*, 10, 907-921.

591 Balic Zunic, T. and Vickovic, I. (1996) IVTON- a program for the calculation of geometrical
 592 aspects of crystal structures and some crystal chemical applications. *Journal of Applied*
 593 *Crystallography*, 29, 305-306.

594 Barbanson, L. and Bastos Neto, A.C. (1992) Hydroandradite titanifère fluorée et grenat
 595 ($\text{Spe}_{39}\text{Gro}_{31}\text{Alm}_{23}\text{And}_6$) fluoré des granitoïdes du district à fluorine de Santa Catarina
 596 (Brésil): description minéralogique, mécanisme d'incorporation du fluor, signification
 597 pétrologique et métallogénique. *Comptes Rendus de l'Académie des Sciences, Série II*, 314,
 598 63-69.

599 Basso, R. and Cabella, R. (1990) Crystal chemical study of garnets from metarodingites in the
 600 Voltri Group metaophiolites (Ligurian Alps, Italy). *Neues Jahrbuch für Mineralogie*
 601 *Monatshefte*, 1990, 127-136.

602 Basso, R., Cimmino, F., and Messiga, B. (1984a) Crystal chemistry of hydrogarnets from three
 603 different microstructural sites of a basaltic metarodingite from the Voltri Massif (Western
 604 Liguria, Italy). *Neues Jahrbuch für Mineralogie Abhandlungen*, 148, 246-258.

605 Basso, R., Cimmino, F., and Messiga, B. (1984b) Crystal chemical and petrological study of
 606 hydrogarnets from a Fe-gabbro metarodingite (Gruppo di Voltri, Western Liguria, Italy). *Neues*
 607 *Jahrbuch für Mineralogie Abhandlungen*, 150, 247-258.

608 Bell, D.R., Rossman, G.R., and Moore, R.O. (2004) Abundance and partitioning of OH in a high-
 609 pressure magmatic system: megacrysts from the Monastery kimberlite, South Africa. *Journal of*
 610 *Petrology*, 45(8), 1539-1564.

611 Betteridge, P.W., Carruthers, J.R., Cooper, R.I., Prout, K., and Watkin, D.J. (2003) Crystals version
 612 12: software for guided crystal structure analysis. *Journal of Applied Crystallography*, 36, 1487.

613 Born, L. and Zemmann, J. (1964) Abstandsberechnungen und gitterenergetische Berechnungen an
 614 Granaten. *Contributions to Mineralogy and Petrology*, 10, 2-23.

615 Brod, J.A., Junqueira-Brod, T.C., Gaspar, J.C., Gibson, S.A., and Thompson, R.N. (2003) Ti-rich
616 and Ti-poor garnet from the Tapira carbonatite complex, SE Brazil: fingerprinting fractional
617 crystallization and liquid immiscibility. In 8th International Kimberlite Conference, Extended
618 Abstracts (CD), FLA_0399.pdf, p. 5.

619 Bruker (2003a) COSMO (Version 1.61), Bruker AXS Inc., Madison, Wisconsin, USA.

620 Bruker (2003b) SAINT (Version 7.60A). Bruker AXS Inc., Madison, Wisconsin, USA.

621 Cempírek, J., Novák, M., Dolníček, Z., Kotková, J., and Škoda, R. (2010) Crystal chemistry and
622 origin of grandidierite, ominelite, boralsilite, and werdingite from the Bory Granulite Massif,
623 Czech Republic. *American Mineralogist*, 95, 1533-1547.

624 Chakhmouradian, A.R. and McCammon, C.A. (2005) Schorlomite: a discussion of the crystal
625 chemistry, formula, and inter-species boundaries. *Physics and Chemistry of Minerals*, 32, 277-
626 289.

627 Chakhmouradian, A.R., Cooper, M.A., Medici, L., Hawthorne, F.C., and Adar, F. (2008) Fluorine-
628 rich hibschite from silicocarbonatite, Afrikanda complex, Russia: crystal chemistry and
629 conditions of crystallization. *Canadian Mineralogist*, 46, 1033-1042.

630 Cussen, E.J. (2006) The structure of lithium garnets: cation disorder and clustering in a new family
631 of fast Li⁺ conductors. *Chemical Communications*, 4, 412-413.

632 Deer, W.A., Howie, R.A., and Zussman, J. (1982) *Rock-forming minerals, Orthosilicates*, 1A,
633 Longman, New York.

634 Dingwell, D.B. and Brearley, M. (1985) Mineral chemistry of igneous melanite garnets from
635 analcite-bearing volcanic rocks, Alberta, Canada. *Contributions to Mineralogy and Petrology*,
636 90, 29-35.

637 Dwarzski, R.E., Draper, D.S., Shearer, C.K., and Agee, C.B. (2006). Experimental insights on
638 crystal chemistry of high-Ti garnets from garnet-melt partitioning of rare-earth and high-field-
639 strength elements. *American Mineralogist*, 91(1), 1536-1546.

640 Dyar, M.D., Schaefer, M.W., Sklute, E.C., and Bishop, J.L. (2008): Mössbauer spectroscopy of
 641 phyllosilicates: effect of fitting models on recoil-free fractions and redox ratios. *Clay Minerals*,
 642 43, 3-33.

643 Dyar, M.D., Breves, E.A., Emerson, E., Bell, S.W., Nelms, M., Ozanne, M.V., Pell, S.E.,
 644 Carmosino, M.L., Tucker, J.M., Gunter, M.E., Delaney, J.S., Lanzirrotti, A., and Woodland, A.B.
 645 (2012) Accurate determination of ferric iron in garnets by bulk Mössbauer spectroscopy and
 646 synchrotron micro-XANES. *American Mineralogist*, 97(10), 1726-1740.

647 Eeckhout, S.G., Castañeda, C., Ferreira, A.C.M., Sabioni, A.C.S., de Grave, E., and Vasconcelos,
 648 D.C.L. (2002) Spectroscopic studies of spessartine from Brazilian pegmatites. *American*
 649 *Mineralogist*, 87, 1297-1306.

650 Faryad, S.W. and Dianiška, I. (2003) Ti-bearing andradite-prehnite-epidote assemblage from the
 651 Malá Fatra granodiorite and tonalite (Western Carpathians). *Schweizerische Mineralogische und*
 652 *Petrographische Mitteilugen*, 83, 47-56.

653 Ferro, O., Galli, E., Papp, G., Quartieri, S., Szakáll, S., and Vezzalini, G. (2003) A new occurrence
 654 of katoite and re-examination of the hydrogrossular group. *European Journal of Mineralogy*, 15,
 655 419-426.

656 Flohr, M.J.K. and Ross, M. (1989) Alkaline igneous rocks of Magnet Cove, Arkansas:
 657 Metasomatized ijolite xenoliths from Diamond Jo quarry. *American Mineralogist*, 74, 113-131.

658 Freiburger, R., Hecht, L., Cuney, M., and Morteani, G. (2001) Secondary Ca-Al silicates in plutonic
 659 rocks: implications for their cooling history. *Contribution to Mineralogy and Petrology*, 141,
 660 415-429.

661 Galuskin, E.V. (2005) Minerals of the vesuvianite group from the achtarandite rocks (Wiluy River,
 662 Yakutia), 191 p. University of Silesia Publishing House, Katowice, Poland (in Polish).

663 Galuskina, I.O., Galuskin, E.V., Armbruster, T., Lazic, B., Kusz, J., Dzierżanowski, P., Gazeev,
 664 V.M., Pertsev, N.N., Prusik, K., Zadov, A.E., Winiarski, A., Wrzalik, R., and Gurbanov, A.G.

665 (2010a) Elbrusite-(Zr) - A new uranian garnet from the Upper Chegem caldera, Kabardino-
 666 Balkaria, Northern Caucasus, Russia. *American Mineralogist*, 95, 1172-1181.

667 Galuskina, I.O., Galuskin, E.V., Armbruster, T., Lazic, B., Dzierzanowski, P., Gazeev, V.M.,
 668 Prusik, K., Pertsev, N.N., Winiarski, A., Zadov, A.E., Wrzalik, R., and Gurbanov, A.G. (2010b)
 669 Bitikleite-(SnAl) and bitikleite-(ZrFe): New garnets from xenoliths of the Upper Chegem
 670 volcanic structure, Kabardino-Balkaria, Northern Caucasus, Russia. *American Mineralogist*, 95,
 671 959-967.

672 Geiger, C.A. (2013) Garnet: a key phase in nature, the laboratory and technology. *Elements*, 9(6),
 673 447-452.

674 Geller, S. (1971) Refinement of the crystal structure of cryolithionite, $\{Na_3\}[Al_2](Li_3)F_{12}$. *American*
 675 *Mineralogist*, 56, 18-23.

676 Grew, E.S., Chernosky, J.V., Werding, G., Abraham, K., Marquez, N., and Hinthorne, J.R. (1990)
 677 Chemistry of kornepine and associated minerals, a wet chemical, ion microprobe, and X-ray
 678 study emphasizing Li, Be, B and F contents. *Journal of Petrology*, 31(5), 1025-1070.

679 Grew, E.S., Locock, A.J., Mills, S.J., Galuskina, I.O., Galuskin, E.V., and Hålenius, U. (2013)
 680 Nomenclature of the Garnet Supergroup. *American Mineralogist*, 98, 785-811.

681 Guascito, M.R., Mesto, E., Malitesta, C., Picca, R.A. and Scordari, F. (2014) The effect of XPS
 682 background removing method on the appraisal of Ti and Fe: The case of phlogopites and
 683 brookite. *American Mineralogist*, 99(1), 139-148.

684 Gwalani, L.G., Rock, N.M.S., Ramasamy, R., Griffin, B.J., and Mulai, B.P. (2000) Complexly
 685 zoned Ti-rich melanite-schorlomite garnets from Ambadungar carbonatite-alkalic complex,
 686 Deccan Igneous Province, Gujarat State, Western India. *Journal of Asian Earth Sciences*, 18,
 687 163-176.

688 Howie, R.A. and Woolley, A.R. (1968) The role of titanium and the effect of TiO₂ on the cell-size,
689 refractive index, and specific gravity in the andradite-melanite-schorlomite series. *Mineralogical*
690 *Magazine*, 36, 775-790.

691 Höfer, H.E. and Brey, G.P. (2007) The iron oxidation state of garnet by electron microprobe: Its
692 determination with the flank method combined with major-element analysis. *American*
693 *Mineralogist*, 92, 873-885.

694 Huggins, F.E., Virgo, D., and Huckenholz, H.G. (1977a) Titanium-containing silicate garnets. I.
695 The distribution of Al, Fe³⁺, and Ti⁴⁺ between octahedral and tetrahedral sites. *American*
696 *Mineralogist*, 62, 475-490.

697 Huggins, F.E., Virgo, D., and Huckenholz, H.G. (1977b) Titanium-containing silicate garnets. II.
698 The crystal chemistry of melanites and schorlomite. *American Mineralogist*, 62, 646-655.

699 Kalinichenko, A.M., Proshko, V.Ya., Matiash, I.V., Pavlishin, V.I., and Garmanik, M.Ya. (1987)
700 NMR data on crystallochemical features of hydrogrossular. *Geochemistry International*, 24(4),
701 132-135 (translated from *Geokhimiya*, 9, 1363-1366, 1986).

702 Katerinopoulou, A., Katerinopoulos, A., Voudouris, P., Bieniok, A., Musso, M., and Amthauer, G.
703 (2009) A multi-analytical study of the crystal structure of unusual Ti-Zr-Cr-rich Andradite from
704 the Maronia skarn, Rhodope massif, western Thrace, Greece. *Mineralogy and Petrology*, 95,
705 113-124.

706 Koga, K., Hauri, E., Hirschmann, M., Bell, D. (2003) Hydrogen concentration analyses using SIMS
707 and FTIR: Comparison and calibration for nominally anhydrous minerals. *Geochemistry*
708 *Geophysics Geosystems*, 4(2), 1-20.

709 Kühberger, A., Fehr, T., Huckenholz, H.G., and Amthauer, G. (1989) Crystal chemistry of a natural
710 schorlomite and Ti-andradites synthesized at different oxygen fugacities. *Physics and Chemistry*
711 *of Minerals*, 16, 734-740.

712 Lagarec, K. and Rancourt, D.G. (1997) Extended Voigt-based analytic lineshape method for
 713 determining *N*-dimensional correlated hyperfine parameter distributions in Mössbauer
 714 spectroscopy. Nuclear Instruments and Methods in Physics Research B, 129, 266-280.

715 Lagarec, K. and Rancourt, D.G. (1998) RECOIL, Mössbauer Spectral Analysis Software for
 716 Windows (version 1.0). Department of Physics, University of Ottawa, Canada.

717 Lager, G.A., Armbruster, T., and Faber, J. (1987) Neutron and X-ray diffraction study of
 718 hydrogarnet $\text{Ca}_3\text{Al}_2(\text{O}_4\text{H}_4)_3$. American Mineralogist, 72, 756-765.

719 Lager, G.A., Armbruster, T., Rotella, F.J., and Rossman, G.R. (1989) OH substitution in garnets: X-
 720 ray and neutron diffraction, infrared, and geometric-modeling studies. American
 721 Mineralogist, 74, 840-851.

722 Locock, A., Luth, R.W., Cavell, R.G., Smith, D.G.W., and Duke, M.J.M. (1995) Spectroscopy of
 723 the cation distribution in the schorlomite species of garnet. American Mineralogist, 80, 27-38.

724 Lupini, L., Williams, C.T., and Wooley, A.R. (1992) Zr-rich garnet and Zr- and Th-rich perovskite
 725 from the Polino carbonatite, Italy. Mineralogical Magazine, 56, 581-586.

726 Malaspina, N., Poli, S., and Fumagalli, P. (2009) The oxidation state of metasomatized mantle
 727 wedge: insights from C–O–H-bearing garnet peridotite. Journal of Petrology, 50, 1533-1552.

728 Malaspina, N., Langenhorst, F., Fumagalli, P., Tumati, S., and Poli, S. (2012) Fe^{3+} distribution
 729 between garnet and pyroxenes in mantle wedge carbonate-bearing garnet peridotites (Sulu,
 730 China) and implications for their oxidation state. Lithos, 146-147, 11-17.

731 Maldener, J., Hösch, A., Langer, K., and Rauch, F. (2003) Hydrogen in some natural garnets
 732 studied by nuclear reaction analysis and vibrational spectroscopy. Physics and Chemistry of
 733 Minerals, 30, 337-344.

734 Malitesta, C., Losito, I., Scordari, F., and Schingaro, E. (1995) XPS investigation of titanium in
 735 melanites from Monte Vulture (Italy). European Journal of Mineralogy, 7, 847-858.

736 Manning, C.E. and Bird, D.K. (1990) Fluorian garnets from the host rocks of the Skaergaard
737 intrusion: implications for metamorphic fluid composition. *American Mineralogist*, 75, 859-873.

738 Matthews, M., Harte, B., and Prior, D. (1992) Mantle garnets: A cracking yarn. *Geochimica et*
739 *Cosmochimica Acta*, 56(7), 2633-2642.

740 Merli, M., Callegari, A., Cannillo, E., Caucia, F., Leona, M., Oberti, R., and Ungaretti, L. (1995)
741 Crystal-chemical complexity in natural garnets: structural constraints on chemical variability.
742 *European Journal of Mineralogy*, 7, 1239-1249.

743 Müntener, O. and Hermann, J. (1994) Titanian andradite in a metapyroxenite layer from the
744 Malenco ultramafics (Italy): implications for Ti-mobility and low oxygen fugacity. *Contribution*
745 *to Mineralogy and Petrology*, 116, 156-168.

746 Novak, G.A. and Gibbs, G.V. (1971) The crystal chemistry of the silicate garnets. *American*
747 *Mineralogist*, 56, 791-825.

748 Onuki, H., Akasaka, M., Yoshida, T., and Nedachia, M. (1982) Ti-Rich Hydroandradites from the
749 Sanbagawa Metamorphic Rocks of the Shibukawa Area, Central Japan. *Contribution to*
750 *Mineralogy and Petrology*, 80, 183-188.

751 Ortalli, I., Pedrazzi, G., Schingaro, E., and Scordari, F. (1994) Iron site populations from Mössbauer
752 spectroscopy in Ti-bearing garnets from Mt. Vulture (Italy). *Hyperfine Interactions*, 91, 727-732.

753 Ottolini, L. and Hawthorne, F.C. (2001) SIMS ionization of hydrogen in silicates: a case study of
754 kornerupine. *Journal of Analytical Spectrometry*, 16, 1266-1270.

755 Ottolini, L., Bottazzi, P., Zanetti, A., and Vannucci, R. (1995) Determination of Hydrogen in
756 Silicates by Secondary Ion Mass Spectrometry. *The Analyst*, 120, 1309-1313.

757 Ottolini, L., Camara, F., Hawthorne, F.C., and Stirling, J. (2002) SIMS matrix effects in the analysis
758 of light elements in silicate minerals: Comparison with SREF and EMPA data. *American*
759 *Mineralogist*, 87, 1477-1485.

760 Pedrazzi, G., Schingaro, E., and Scordari, F. (1998) X-ray single crystal and Mössbauer study on
 761 Ti-garnets from the Tapira alkaline-carbonatite complex, Brazil. In E.B. Saitovitch, H.
 762 Rechenberg, and R.B. Scorzelli, Eds., *Hyperfine Interactions (C)*, 3, 321-324.
 763 Pedrazzi, G., Schingaro, E., and Scordari, F. (2002) Mössbauer investigation on Ti-garnets from
 764 different geological environments. In M.F. Thomas, J.M. Williams, and T.C. Gibb, Eds.,
 765 *Hyperfine Interactions (C)*, 5, 457-460.
 766 Phichaikamjornwut, B., Skogby, H., Ounchanum, P., Limtrakun, P., and Boonsoong, A. (2011)
 767 Hydrous components of grossular-andradite garnets from Thailand: thermal stability and
 768 exchange kinetics. *European Journal of Mineralogy*, 24, 107-121.
 769 Platt, R.G. and Mitchell, R.H. (1979) The Marathon Dikes. I: Zirconium-rich titanian garnets and
 770 manganoan magnesian ulvöspinel-magnetite spinels. *American Mineralogist*, 64, 546-550.
 771 Robinson, K., Gibbs, G.V., and Ribbe, P.H. (1971) Quadratic Elongation: A Quantitative Measure
 772 of Distortion in Coordination Polyhedra. *Science*, 172, 567-570.
 773 Rossman, G.R. and Aines, R.D. (1991) The hydrous components in garnets: Grossular-
 774 hydrogrossular. *American Mineralogist*, 76, 1153-1164.
 775 Saha, A., Ray, J., Ganguly, S., and Chatterjee, N. (2011) Occurrence of melanite garnet in syenite
 776 and ijolite-melteigite rocks of Samchampi-Samteran alkaline complex, Mikir Hills, Northeastern
 777 India. *Current Science*, 101(1), 95-100.
 778 Schingaro, E., Scordari, F., Capitanio, F., Parodi, G., Smith, D., and Mottana, A. (2001) Crystal
 779 chemistry of kimzeyte from Anguillara, Mts. Sabatini, Italy. *European Journal of Mineralogy*,
 780 13, 749-759.
 781 Schingaro, E., Scordari, F., Pedrazzi, G., and Malitesta, C. (2004) Ti and Fe speciation by X-ray
 782 Photoelectron Spectroscopy (XPS) and Mössbauer Spectroscopy for a full crystal chemical
 783 characterisation of Ti-garnets from Colli Albani (Italy). *Annali di chimica*, 94, 185-196.

784 Scordari, F., Schingaro, E., and Pedrazzi, G. (1999) Crystal chemistry of melanite from Mt. Vulture
785 (Southern Italy). *European Journal of Mineralogy*, 11, 855-869.

786 Scordari, F., Dyar, M.D., Schingaro, E., Lacalamita, M., and Ottolini, L. (2010) XRD, micro-
787 XANES, EMPA, and SIMS investigation on phlogopite single crystals from Mt. Vulture (Italy).
788 *American Mineralogist*, 95, 1657-1670.

789 Shannon, R.D. (1976) Revised effective ionic radii and systematic studies of interatomic distances
790 in halides and chalcogenides. *Acta Crystallographica*, A32, 751-767.

791 Sheldrick, G.M. (2003) SADABS, Program for Empirical Absorption Correction of Area Detector
792 Data. University of Göttingen, Germany.

793 Shenoy, G.K., Wagner, F.E., and Kalvius, G.M. (1978) The measurement of the isomer shift. In
794 G.K. Shenoy and F.E. Wagner, Eds., *Mössbauer Isomer Shifts*, p. 49-110. Amsterdam: North-
795 Holland Publishing Co.

796 Toby, B.H. and Von Dreele, R.B. (2013) GSAS-II: the genesis of a modern open-source all purpose
797 crystallography software package. *Journal of Applied Crystallography*, 46(2), 544-549.

798 Ulrych, J., Povondra, P., Pivec, E., Rutšek, J., and Sitek, J. (1994) Compositional evolution of
799 metasomatic garnet in melilitic rocks of the Osečná complex, Bohemia. *Canadian Mineralogist*,
800 32, 637-647.

801 Ungaretti, L., Leona, M., Merli, M., and Oberti, R. (1995) Non-ideal solid-solution in garnet:
802 crystal-structure evidence and modelling. *European Journal of Mineralogy*, 7, 1299-1312.

803 Valley, J.W., Essene, E.J., and Peacor, D.R. (1983) Fluorine-bearing garnets in Adirondack calc-
804 silicates. *American Mineralogist*, 68, 444-448.

805 Visser, D. (1993) Fluorine-bearing hydrogarnets from Blengsvatn, Bamble sector, south Norway.
806 *Mineralogy and Petrology*, 47, 209-218.

807 Wang, Y. and Lai, W. (2012) High ionic conductivity lithium garnet oxides of $\text{Li}_{7-x}\text{La}_3\text{Zr}_{2-x}\text{Ta}_x\text{O}_{12}$
808 compositions. *Electrochemical and Solid-State Letters*, 15(5), A68-A71.

- Watkin, D. (2008) Structure refinement: some background theory and practical strategies. *Journal of Applied Crystallography*, 41, 491-522.
- Waychunas, G.A. (1987) Synchrotron radiation XANES spectroscopy of Ti in minerals: Effects of Ti bonding distances, Ti valence, and site geometry on absorption edge structure. *American Mineralogist*, 72, 89-101.
- Wood, B.J., Kiseeva, E.S., and Matzen, A.K. (2013) Garnet in the Earth's mantle. *Elements*, 9, 421-426.
- Yang, H., Konzett, J., Downs, R.T., and Frost, D.J. (2009) Crystal structure and Raman spectrum of a high-pressure Li-rich majoritic garnet, $(\text{Li}_2\text{Mg})\text{Si}_2(\text{SiO}_4)_3$. *American Mineralogist*, 94, 630-633.
- Young, R.A., Ed. (1993) *The Rietveld method*, 308 p. International Union of Crystallography, Oxford Science Publications.

FIGURE CAPTIONS

FIGURE 1. Plot of the TiO_2 (wt%) vs. measured H_2O (wt%) in Ti-garnets. Symbols: solid squares = samples of this work; open symbols = samples from literature (circle: 80802 and 80303 from Onuki et al. (1982); pointing downward triangle: SB-3 from Lager et al. (1989); pointing upward triangle: SA12 from Müntener and Hermann (1994); diamond: 31/B from Ulrych et al. (1994); circle with horizontal line: Ice River crystal from Locock et al. (1995); pointing downward triangle with horizontal line: AF-05 from Chakhmouradian and McCammon (2005); pointing upward triangle with horizontal line: M-1 from Katerinopoulou et al. (2009); diamond with horizontal line: KPK39-1-1, KPK54-10, KPK54-11, KTK05, KTK07, KTK09, KTK10, KPK56-12-2, KPK56-12-9, KPN09, KPN10, KPN11 from Phichaikamjornwut et al. (2011)).

FIGURE 2. Room temperature Mössbauer spectra of samples W6 (a) and W16 (b).

834 **FIGURE 3.** Comparison between $\text{Fe}^{3+}/\Sigma\text{Fe}$ as determined by Mössbauer spectroscopy and Flank
835 method. The 1:1 line is shown . The error bars for $\text{Fe}^{3+}/\Sigma\text{Fe}$ correspond respectively to $\sigma = 3\%$ for
836 the Flank method (Malaspina et al. 2012) and $\sigma = 3\%$, the latter being the maximum error for
837 Mössbauer data (Dyar et al. 2008).

838 **FIGURE 4.** XRD patterns of the W6, W12, W16 and NZALA samples.

839 **FIGURE 5.** Splitting of selected diffraction peaks, (004) and (024), from the patterns in **Figure 4**.

840 **FIGURE 6.** Plot of a cell parameter vs. TiO_2 (wt%) in Ti-garnets. Symbols as in **Figure 1**. In
841 addition, circle with vertical line indicates the Magnet Cove andradite from Antao (2013).

842 **FIGURE 7.** Plot of a cell parameter vs. $\langle\text{X-O}\rangle$ (a), Y-O (b) and Z-O (c) distances of Ti-garnets.
843 Symbols as in **Figure 6**.

844 **FIGURE 8.** Plot of tetrahedral angle variance (TAV parameter) vs. $(\text{Fe}^{2+}+\text{Al}+\text{Fe}^{3+}+\text{Ti})$ amount in
845 the tetrahedral site of Ti-garnets and natural end-member garnets. Symbols as in **Figure 6**. Other
846 symbols: circle with cross inside = Novak and Gibbs (1971); square with cross inside = Scordari et
847 al. (1999); pointing downward triangle with cross inside = Schingaro et al. 2001; pointing upward
848 triangle with cross inside = Adamo et al. (2011); diamond with cross inside = Antao (2014).

849 **FIGURE 9.** Plot of octahedral angle variance (OAV parameter) vs. $(\text{Ti}^{4+}+\text{Zr}+\text{Fe}^{2+}+\text{Mg}+\text{Mn}+\text{Ca})$
850 amount in the octahedral site of Ti-garnets and natural end-member garnets. Symbols as in **Figure**
851 **8**.

852 **FIGURE 10.** Classification diagram for the studied and selected literature hydrogarnets. Symbols
853 as in **Figure 8**. Grey symbols indicate the studied samples whose formulae have been calculated
854 according to Grew et al. (2013). In addition, square with horizontal line represents GA34, GRR134,
855 GRR169, GRR684, GRR1328, GRR1765, GA32, GA35, GRR149, GRR1015, GRR1447, GA24,
856 GA36, GRR1446, CITH3110 samples from Amthauer and Rossman (1998).

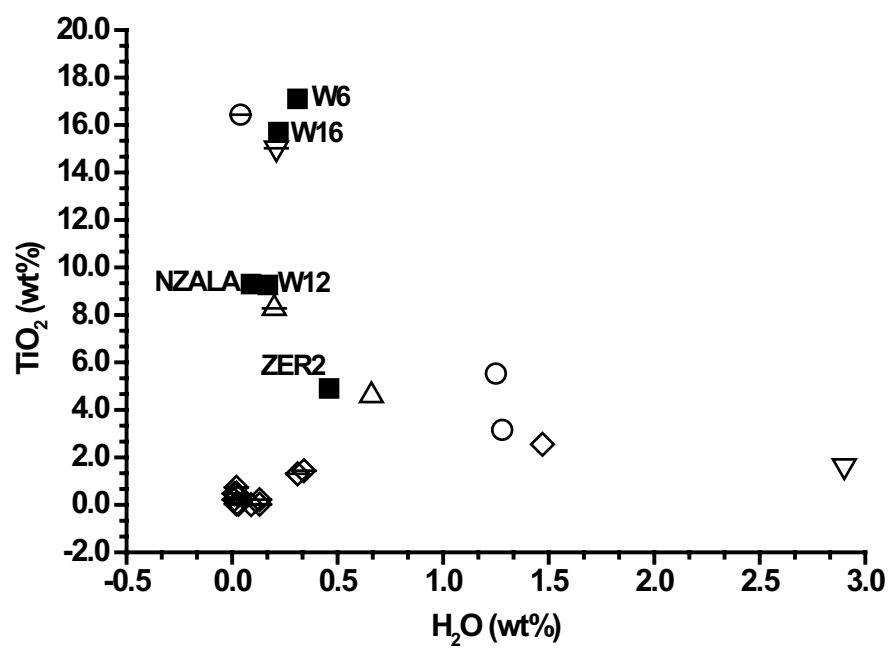


Figure 1

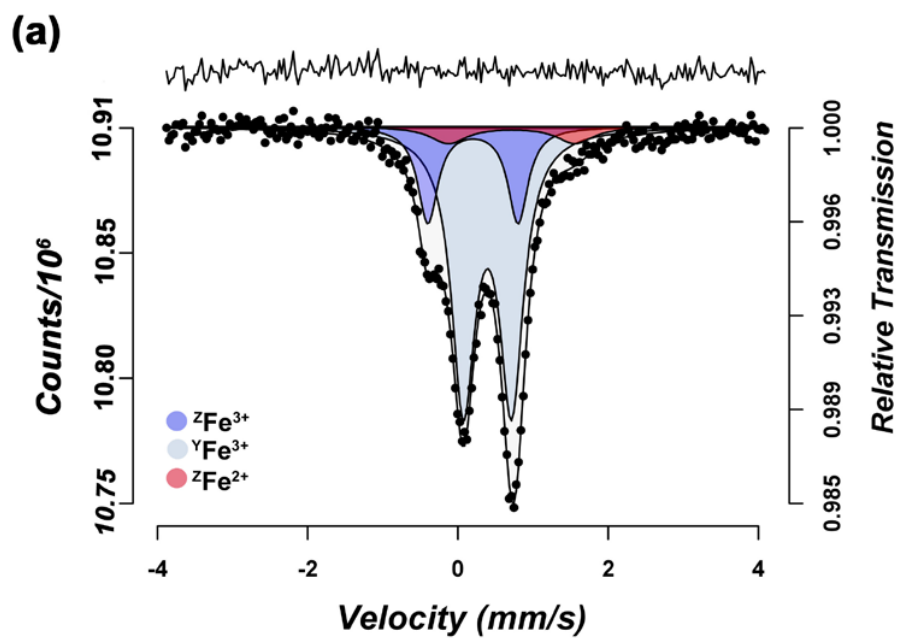


Figure 2a

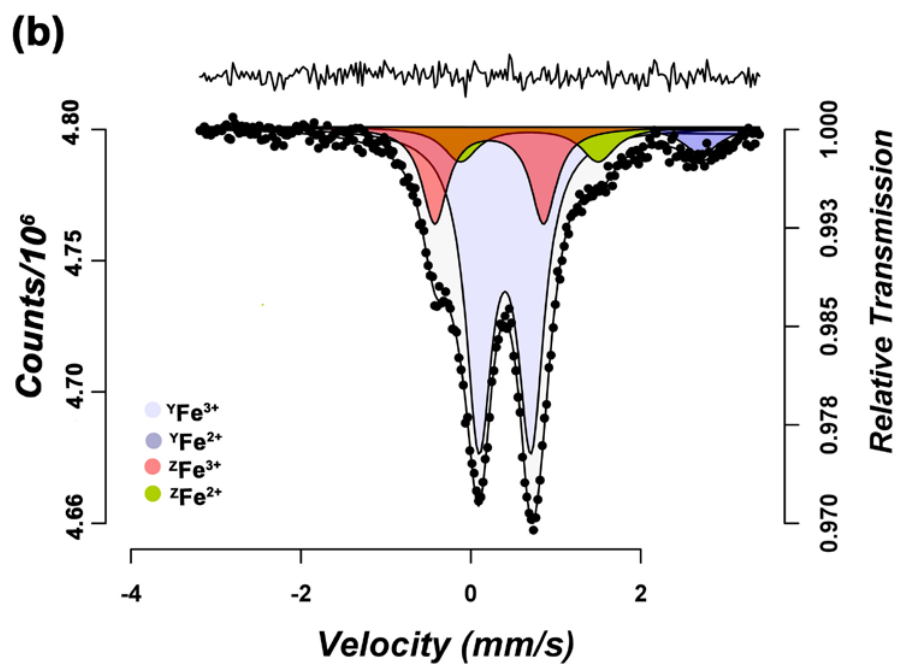


Figure 2b

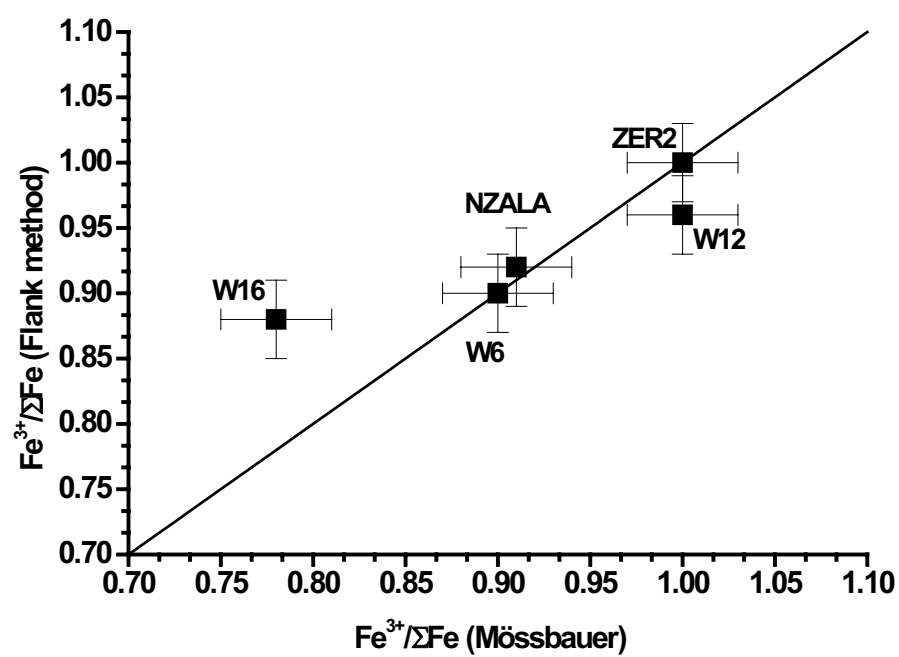


Figure 3

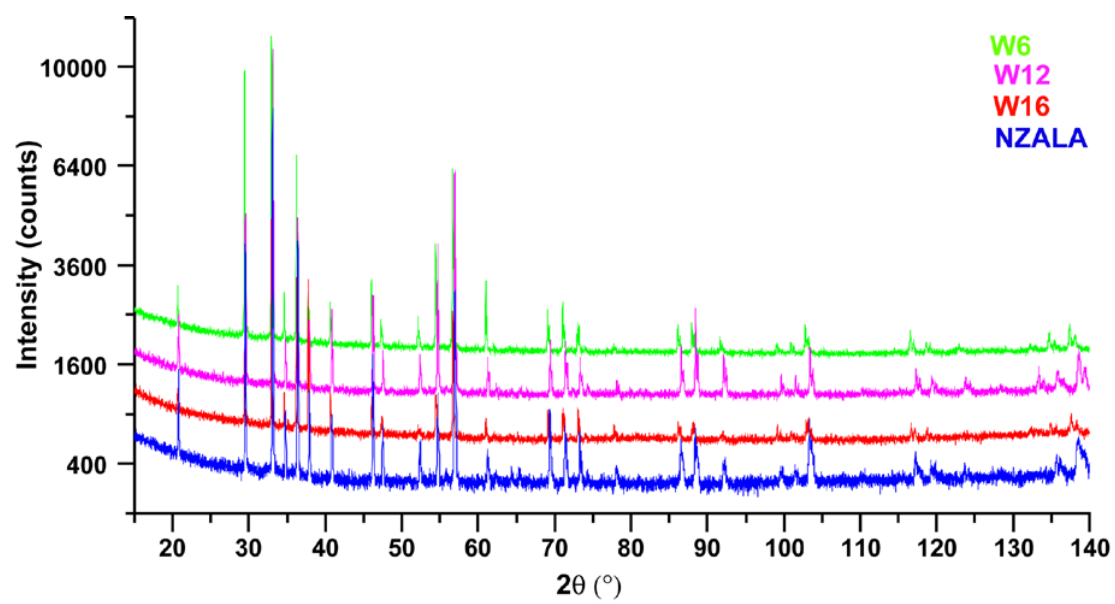


Figure 4

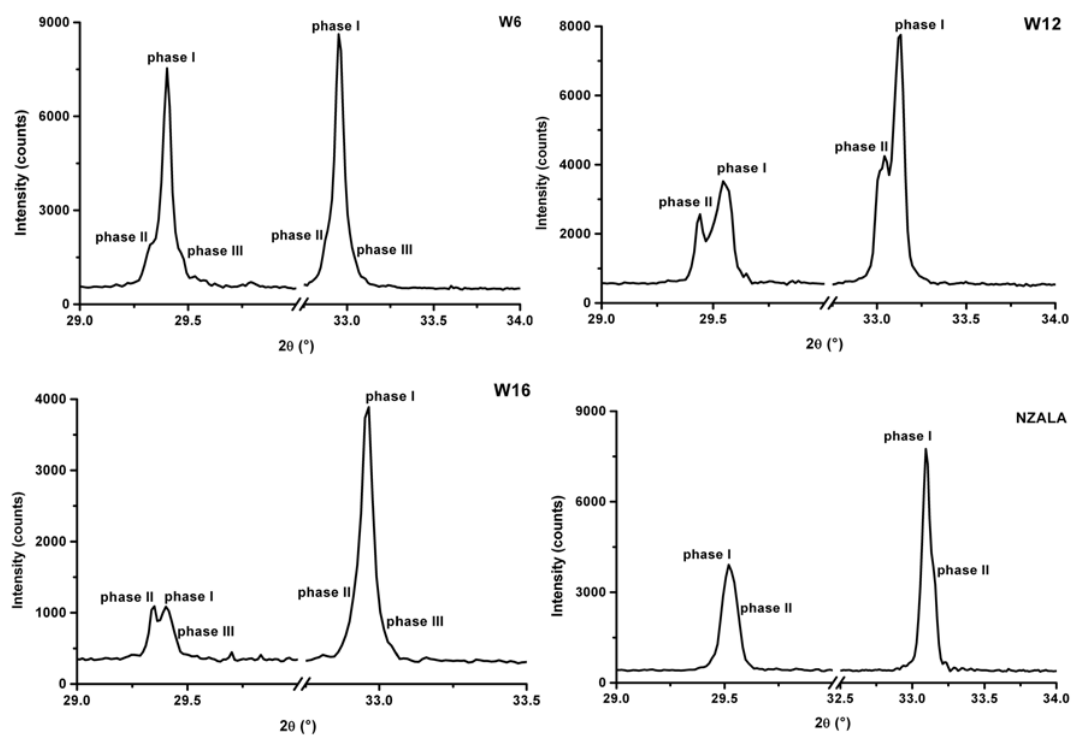


Figure 5

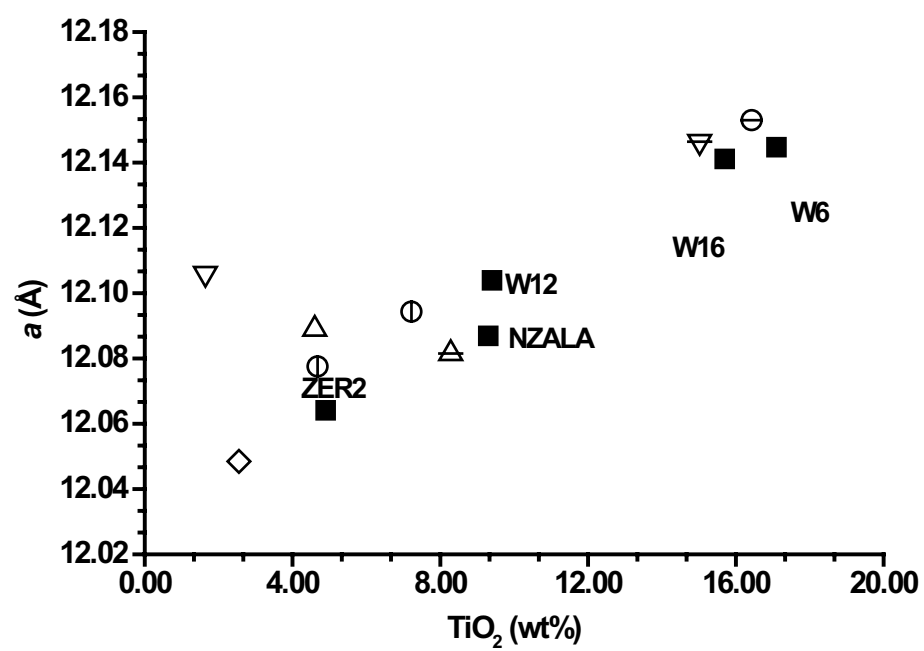


Figure 6

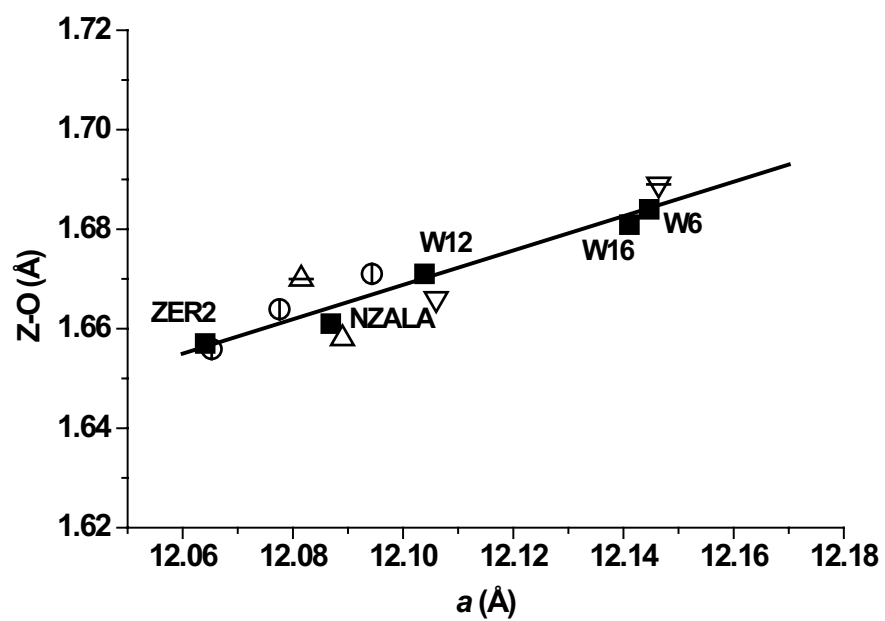


Figure 7a

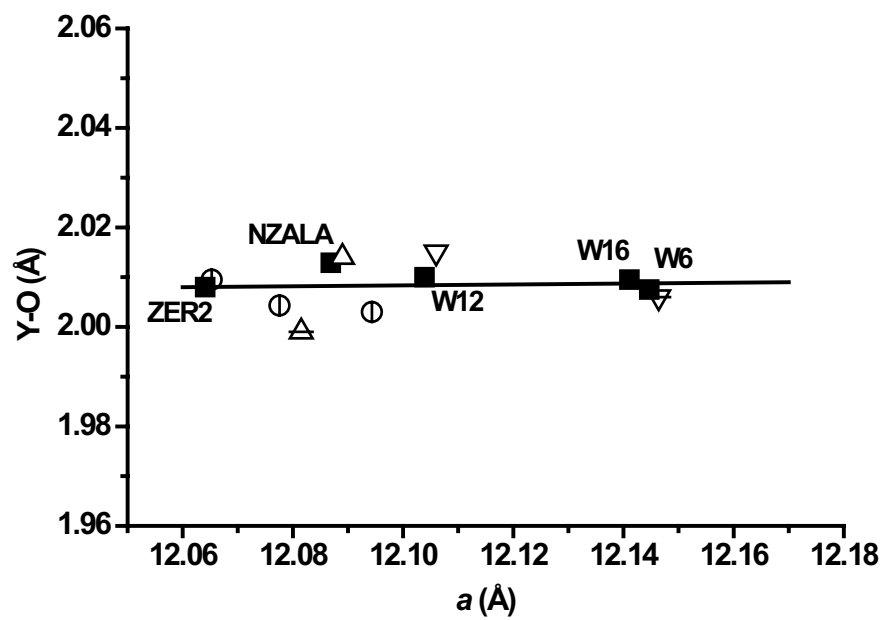


Figure 7b

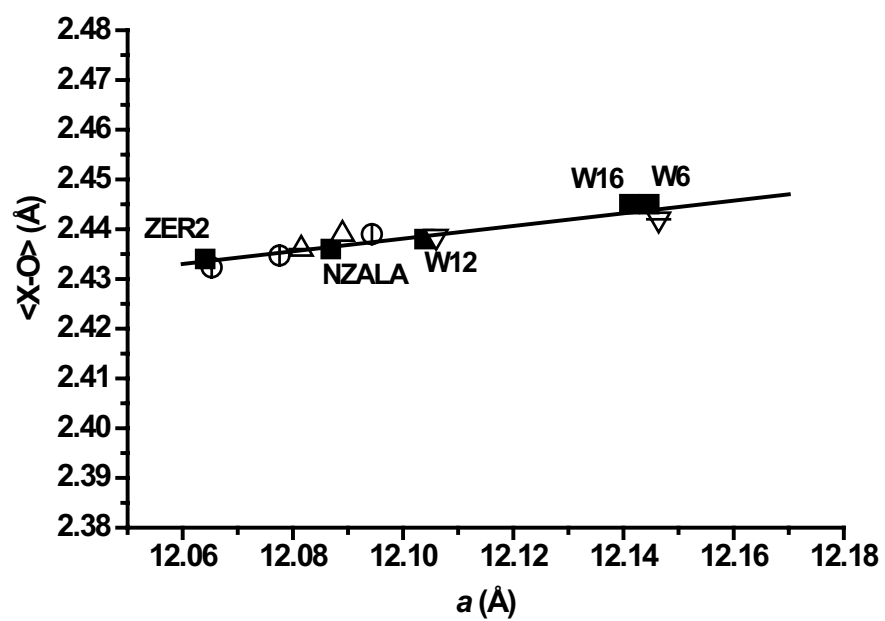


Figure 7c

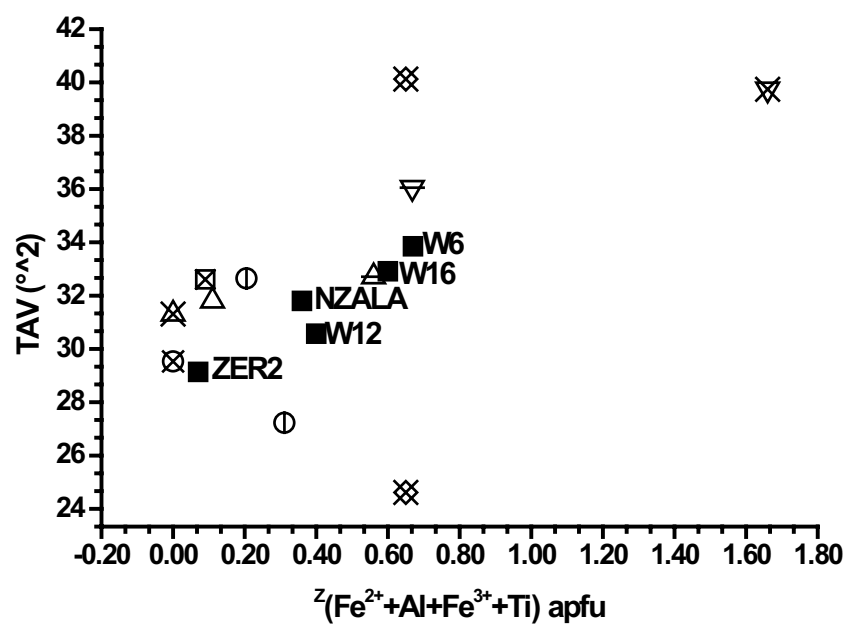


Figure 8

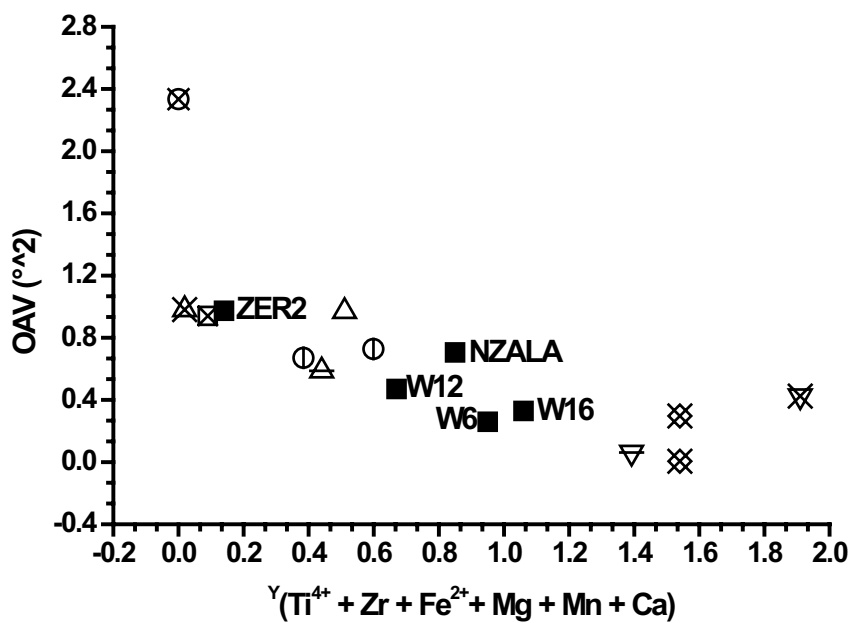


Figure 9

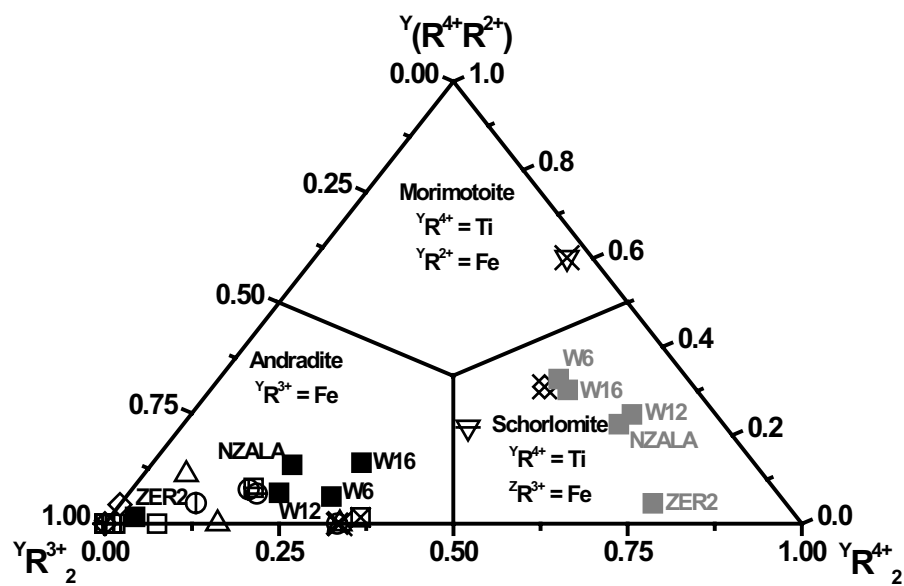


Figure 10

Table 1. Origin, provenance and literature data of the analysed samples.

Label	Provenance	References
Magmatic alkaline rocks		
W6	Iivaara, Finland	Howie and Woolley (1968)
W16	Rusinga Island, Kenya	Howie and Woolley (1968)
Carbonatitic rocks		
W12	Magnet Cove, Arkansas	Howie and Woolley (1968); Pedrazzi et al. (2002)
Metamorphic rocks		
NZALA	Atlas mountains, Marocco	Armbruster et al. (1998); Pedrazzi et al. (2002)
ZER2	Zermatt, Switzerland	Armbruster et al. (1998); Pedrazzi et al. (2002)

Table 2. Chemical composition (wt%) of the studied garnets.

	W6	W12	W16	NZALA	ZER2
CaO	31.7(1)	32.2(1)	31.5(1)	31.9(1)	33.2(1)
Na₂O	0.31(2)	0.05(3)	0.35(2)	0.14(2)	0.01(1)
MgO	1.20(2)	0.99(1)	0.95(3)	0.75(2)	0.44(3)
MnO	0.21(2)	0.26(3)	0.33(2)	0.51(2)	0.23(3)
FeO	19.3(2)	20.1(1)	19.7(2)	20.8(3)	20.9(2)
Al₂O₃	0.96(2)	2.08(4)	1.0(1)	1.17(4)	2.5(1)
ZrO₂	0.18(2)	0.01(1)	0.37(3)	0.2(1)	0.15(1)
TiO₂	17.1(2)	9.26(2)	15.7(1)	9.3(3)	4.9(1)
Cr₂O₃	0.02(1)	0.02(2)	0.01(1)	0.07(3)	0.13(4)
SiO₂	27.0(1)	29.9(1)	27.9(1)	30.4(2)	34.5(4)
Total	98.0(2)	94.9(3)	97.8(2)	95.2(4)	97.0(4)
H₂O[†]	0.31(3)	0.17(1)	0.22(3)	0.091(7)	0.46(4)
Li₂O[†]	0.004(2)	0.0038(2)	0.011(6)	0.008(1)	0.014(2)
F[†]	0.009(4)	0.011(2)	0.040(4)	0.020(1)	0.004(1)
Fe³⁺/ΣFe*	0.90(1)	0.96(1)	0.88(2)	0.92(1)	1.00(1)
Fe³⁺/ΣFe**	0.79	0.96	0.79	0.92	0.86

Note:[†]SIMS data; *from Flank method; **calculated on the basis of the charge balance according to Grew et al. 2013 (see details in the text).

Table 3. Mössbauer parameters of W6 and W16 garnets as obtained by lorentzian fitting and corrected according to Dyar et al. (2012). Literature data on W12, NZALA and ZER2 samples (Pedrazzi et al. 2002) are also reported.

	χ^2_r	Site	Species	IS (mm/s)	QS (mm/s)	Γ (mm/s)	A(%)
W6	0.93	Y	Fe³⁺	0.393(6)	0.64(1)	0.38(1)	70(1)
		Z	Fe³⁺	0.20(1)	1.20(5)	0.32(4)	20(1)
		Z	Fe²⁺	0.7(2)	1.7(7)	0.6(2)	10(2)
		Y	Fe³⁺	0.402(4)	0.61(1)	0.37(8)	59(1)
W16	1.40	Y	Fe²⁺	1.3(7)	2.8(3)	0.52(6)	10(2)
		Z	Fe³⁺	0.22(1)	1.28(6)	0.37(3)	19(3)
		Z	Fe²⁺	0.7(6)	1.6(8)	0.46(6)	12(2)
		Y	Fe³⁺	0.399(5)	0.617(6)	0.326(5)	81(3)
W12*	1.29	Z	Fe³⁺	0.221(2)	1.208(4)	0.401(4)	19(2)
NZALA*	1.11	Y	Fe³⁺	0.402(5)	0.597(5)	0.331(6)	79(7)
		Z	Fe³⁺	0.208(1)	1.253(3)	0.318(4)	12(7)
		Z	Fe²⁺	0.70(1)	1.66(1)	0.25(9)	4(2)
		Y	Fe²⁺	1.28(8)	2.91(2)	0.48(2)	5(3)
ZER2*	1.16	Y	Fe³⁺	0.399(1)	0.582(3)	0.312(4)	100

Notes: χ^2_r = reduced $\chi^2 = \chi^2/\text{degrees of freedom}$; *data from Pedrazzi et al. (2002).

Table 4. Powder and single crystal X-ray diffraction data of the studied garnets.

	W6		W12		W16		NZALA		ZER2
<i>XRPD data</i>									
	phase I	phase II	phase I	phase II	phase I	phase II	phase I	phase II	
Weight fraction (%)	66(3)	34(3)	58(2)	42(2)	81(2)	19(2)	80(2)	20(1)	
<i>a</i> (Å)	12.1476(2)	12.1599(9)	12.0948(3)	12.1156(7)	12.1459(2)	12.1648(9)	12.1045(2)	12.0883(3)	
N _{obs}	148	148	146	148	148	148	148	146	
Data points	10383		10383		10383		10383		
<i>wR</i> (%)	10.45		11.54		10.49		10.12		
<i>SCXRD data</i>									
Crystal size (mm ³)	0.68x0.60x0.25		0.48x0.24x0.16		0.77x0.33x0.07		0.70x0.55x0.14		0.51x0.22x0.11
Space group	<i>Ia</i> $\bar{3}d$		<i>Ia</i> $\bar{3}d$		<i>Ia</i> $\bar{3}d$		<i>Ia</i> $\bar{3}d$		<i>Ia</i> $\bar{3}d$
<i>a</i> (Å)	12.1447(1)		12.1039(1)		12.1411(1)		12.0869(2)		12.0641(1)
Cell volume (Å ³)	1791.27(3)		1773.27(3)		1789.67(3)		1765.81(5)		1755.84(3)
Z	8		8		8		8		8
θ range for data collection	4 to 36°		5 to 30°		4 to 36°		5 to 36°		4 to 36°
Reflections collected	20828		14993		20821		20402		20641
Reflections unique	366		228		366		363		362
R _{merging} [R _(int)] (%)	2.20		2.20		1.93		3.47		1.77
Reflections used (<i>I</i> >3σ(<i>I</i>))	332		206		341		323		334
No. of refined parameters	21		21		21		21		19
Goof*	1.08		0.92		1.02		0.94		0.87
<i>R</i> ₁ [†] [on <i>F</i>] (%)	2.00		1.78		1.95		1.65		2.09
<i>wR</i> ₂ [‡] [on <i>F</i> ²] (%)	2.94		2.38		2.55		2.35		3.02
Δρ _{min} /Δρ _{max} (e [−] /Å ³)	−0.40/0.49		−0.74/0.25		−0.40/0.49		−0.43/0.36		−0.96/0.34

Notes: *: Goodness-of-fit = $[\Sigma(w(F_o^2 - F_c^2)^2)/(N-p)]^{1/2}$, where N and p are the number of reflections and parameters, respectively.

$$^{\dagger}: R_1 = \Sigma[|F_o| - |F_c|]/\Sigma|F_o|.$$
$$^{\ddagger}: wR_2 = [\Sigma[w(F_o^2 - F_c^2)^2]/\Sigma[w(F_o^2)^2]]^{1/2}; w = \text{quasi-unit weight.}$$

Table 5. Crystallographic coordinates, site occupancies, equivalent/isotropic (\AA^2) and anisotropic displacement parameters (\AA^2) of the studied crystals.

Sample	Site	Atom	x	y	z	Occupancy	$U_{\text{iso/equiv}}$	U_{11}	U_{22}	U_{33}	U_{23}	U_{13}	U_{12}
W6													
	X	Ca ²⁺	$\frac{1}{8}$	0	$\frac{1}{4}$	1.0000	0.0087	0.0063(2)	0.0099(1)	0.0099(1)	0.00252(8)	0	0
	Y	Fe ³⁺	0	0	0	0.7304(8)	0.0049	0.0049(1)	0.0049(1)	0.0049(1)	0.00038(4)	0.00038(4)	0.00038(4)
		Al ³⁺				0.2698(8)							
	Z	Si ⁴⁺	$\frac{3}{8}$	0	$\frac{1}{4}$	0.878(1)	0.0054	0.0046(2)	0.0059(2)	0.0059(2)	0	0	0
		Fe ³⁺				0.137(5)							
	O1	O ²⁻	0.03779(5)	0.04819(5)	0.65358(5)	1.0000	0.0106	0.0132(3)	0.0085(2)	0.0091(3)	0.0011(2)	0.0031(2)	0.0016(2)
W12													
	X	Ca ²⁺	$\frac{1}{8}$	0	$\frac{1}{4}$	1.0000	0.0078	0.0058(2)	0.0088(2)	0.0088(2)	0.00214(9)	0	0
	Y	Fe ³⁺	0	0	0	0.732(1)	0.0044	0.0044(2)	0.0044(2)	0.0044(2)	0.00009(5)	0.00009(5)	0.00009(5)
		Al ³⁺				0.268(1)							
	Z	Si ⁴⁺	$\frac{3}{8}$	0	$\frac{1}{4}$	0.935(2)	0.0041	0.0038(3)	0.0043(3)	0.0043(3)	0	0	0
		Fe ³⁺				0.064(1)							
	O1	O ²⁻	0.03825(4)	0.04823(4)	0.65400(4)	1.0000	0.0078	0.0096(3)	0.0073(3)	0.0066(3)	-0.0001(2)	0.0018(2)	-0.0007(2)
W16													
	X	Ca ²⁺	$\frac{1}{8}$	0	$\frac{1}{4}$	1.0000	0.0085	0.0059(1)	0.0099 (1)	0.0099 (1)	0.00279(9)	0	0
	Y	Fe ³⁺	0	0	0	0.728(1)	0.0045	0.0045(1)	0.0045(1)	0.0045(1)	0.00049(5)	0.00049(5)	0.00049(5)
		Al ³⁺				0.272(1)							
	Z	Si ⁴⁺	$\frac{3}{8}$	0	$\frac{1}{4}$	0.859(1)	0.0052	0.0042(2)	0.0057(2)	0.00557(2)	0	0	0
		Fe ³⁺				0.143(5)							
	O1	O ²⁻	0.03793(5)	0.04821(5)	0.65372(5)	1.0000	0.0099	0.0130(3)	0.0087(3)	0.0080(2)	-0.0008(2)	0.00284(2)	-0.0017(2)
NZALA													
	X	Ca ²⁺	$\frac{1}{8}$	0	$\frac{1}{4}$	1.0000	0.0083	0.0062(1)	0.0094(1)	0.0094(1)	0.00202(6)	0	0
	Y	Fe ³⁺	0	0	0	0.7932(9)	0.0050	0.0050(1)	0.0050(1)	0.0050(1)	0.00015(3)	0.00015(3)	0.00015(3)
		Al ³⁺				0.207(1)							

	Z	Si ⁴⁺	⅜	0	¼	0.912(1)	0.0052	0.0045(2)	0.0055(1)	0.0055(1)	0	0	0
	O1	Fe ³⁺				0.071(5)							
	O1	O ²⁻	0.03869(4)	0.04831(4)	0.65454(4)	1.0000	0.0085	0.0098(2)	0.0084(2)	0.0072(2)	-0.0001(1)	0.0010(1)	-0.0004(1)
ZER2	X	Ca ²⁺	⅛	0	¼	1.0000	0.0064	0.0046(2)	0.0074(2)	0.0074(2)	0.00170(7)	0	0
	Y	Fe ³⁺	0	0	0	0.7658(1)	0.0046	0.0046(2)	0.0046(2)	0.0046(2)	0.00006(4)	0.00006(4)	0.00006(4)
	Z	Al ³⁺				0.2344(1)							
	Z	Si ⁴⁺	⅜	0	¼	1.0000	0.0049	0.0043(2)	0.0052(2)	0.0052(2)	0	0	0
	O1	O ²⁻	0.03899(4)	0.04825(4)	0.65457(4)	1.0000	0.0064	0.0070(2)	0.0067(2)	0.0055(2)	0.0000(1)	0.0004(1)	-0.0002(1)

Table 6. Refined bond distances (Å) and distortional parameters of the studied samples, selected literature Ti-garnets and natural end-member garnets.

						Ti-andradite	Ti-andradite	Ti-Zr-Cr-rich Andradite	Ti-rich Andradite			Schorlomite	Andradite	Morimotoite		Grossular	Kimzeyite	Melanite
	W6	W12	W16	NZALA	ZER2	Lager et al. (1989)	Müntener and Hermann (1994)	Katerinopoulou et al. (2009)	Antao (2013) Phase I	Antao (2013) Phase II	Antao (2013) Phase III	Chakhmouradian and McCammon (2005)	Adamo et al. (2011)	Antao (2014) Phase I	Antao (2014) Phase II	Novak and Gibbs (1971)	Schingaro et al. (2001)	Scordari et al. (1999)
X1-O	2.371(1)	2.366(1)	2.371(1)	2.364(1)	2.362(1)	2.369(1)	2.365(1)	2.361(1)	2.3609(8)	2.373(1)	2.3575(8)	2.368(1)	2.3609(7)	2.3631(9)	2.338(3)	2.325(1)	2.409(2)	2.347(1)
X2-O	2.518(1)	2.510(1)	2.517(1)	2.508(1)	2.505(1)	2.508(1)	2.512(1)	2.510(1)	2.5085(9)	2.505(1)	2.5070(8)	2.515(1)	2.5009(6)	2.5134(9)	2.515(3)	2.482(1)	2.546(2)	2.498(1)
<X-O>	2.445(1)	2.438(1)	2.444(1)	2.436(1)	2.434(1)	2.439(1)	2.439(1)	2.436(1)	2.4347(9)	2.439(1)	2.4323(8)	2.442(1)	2.4309(7)	2.4383(9)	2.427(3)	2.404(1)	2.478(2)	2.423(1)
Y-O	2.008(1)	2.008(1)	2.010(1)	2.0121(4)	2.009(1)	2.015(1)	2.014(1)	1.999(1)	2.0043(9)	2.003(1)	2.0095(9)	2.006(1)	2.0199(6)	2.011(1)	1.988(3)	1.924(1)	2.050(2)	1.989(1)
Z-O	1.684(1)	1.671(1)	1.681(1)	1.6615(4)	1.656(1)	1.666(1)	1.658(1)	1.670(1)	1.6639(9)	1.671(1)	1.6559(9)	1.689(1)	1.6474(6)	1.693(1)	1.704(3)	1.645(1)	1.738(2)	1.651(1)
<D-O>[Å]	2.145	2.139	2.145	2.136	2.131	2.140	2.137	2.135	2.134	2.138	2.132	2.145	2.132	2.145	2.136	2.094	2.186	2.121
Volume_x [Å³]	25.019	24.759	25.001	24.705	24.616	24.781	24.790	24.731	24.697	24.773	24.623	24.933	24.528	24.856	25.165	23.800	26.012	24.316
Δ(X-O)	0.147	0.138	0.145	0.143	0.137	0.139	0.146	0.149	0.148	0.133	0.149	0.148	0.140	0.15	0.127	0.1557	0.136	0.152
α (°)	26.518	26.851	26.603	26.888	26.847	26.950	26.771	26.429	26.594	26.710	26.745	26.584	27.213	26.803	26.168	24.871	27.368	26.331
Volume_y [Å³]	10.786	10.816	10.818	10.873	10.791	10.904	10.885	10.652	10.733	10.718	10.815	10.766	10.983	10.847	10.478	9.528	11.507	10.473
OAV [°^2]	0.259	0.47	0.329	0.705	0.973	0.579	0.969	0.580	0.670	0.727	0.800	0.062	0.981	0.005	0.297	2.335	0.424	0.94
S(Y) [Å]	2.851	2.858	2.855	2.867	2.863	2.868	2.871	2.845	2.854	2.853	2.863	2.843	2.880	2.843	2.825	2.754	2.885	2.834
U(Y) [Å]	2.827	2.825	2.828	2.827	2.816	2.831	2.824	2.809	2.815	2.813	2.820	2.831	2.833	2.846	2.799	2.695	2.917	2.789
t_{SY} [Å]	2.298	2.294	2.298	2.292	2.280	2.297	2.287	2.279	2.283	2.280	2.285	2.307	2.293	2.325	2.275	2.175	2.394	2.258
t_{UY} [Å]	2.338	2.347	2.343	2.357	2.357	2.356	2.363	2.338	2.346	2.346	2.355	2.326	2.371	2.320	2.317	2.273	2.343	2.333
X-Y [Å]	3.395	3.383	3.394	3.378	3.372	3.384	3.379	3.377	3.376	3.380	3.372	3.395	3.371	3.398	3.399	3.314	3.464	3.354
φ(°)	133.55	133.42	133.53	133.49	133.64	133.39	133.70	133.81	133.72	133.66	133.64	133.30	133.34	132.87	133.89	135.51	132.00	134.04
Volume_z [Å³]	2.42	2.368	2.408	2.324	2.31	2.348	2.312	2.358	2.336	2.370	2.301	2.441	2.268	2.455	2.516	2.289	2.656	2.286
TAV [°^2]	33.847	30.567	32.915	31.801	29.135	31.102	31.803	32.615	32.648	27.230	33.657	36.048	31.309	40.124	24.615	27.066	39.742	32.610
S(Z) [Å]	2.618	2.605	2.615	2.587	2.586	2.596	2.582	2.598	2.589	2.612	2.575	2.622	2.566	2.621	2.669	2.582	2.691	2.571
U(Z) [Å]	2.813	2.789	2.807	2.773	2.764	2.781	2.768	2.788	2.779	2.785	2.766	2.824	2.750	2.835	2.837	2.753	2.909	2.759
t_{SZ} [Å]	2.118	2.094	2.112	2.085	2.073	2.089	2.081	2.097	2.090	2.085	2.083	2.130	2.066	2.145	2.118	2.060	2.201	2.075
t_{UZ} [Å]	1.851	1.842	1.849	1.829	1.828	1.836	1.826	1.837	1.831	1.847	1.821	1.854	1.815	1.853	1.887	1.826	1.903	1.818
X-Z [Å]	3.036	3.026	3.035	3.022	3.016	3.027	3.022	3.020	3.019	3.024	3.016	3.037	3.015	3.039	3.040	2.964	3.099	3.000

Notes: <D-O> = [(Z-O) + (Y-O) + (X1-O) + (X2-O)]/4 according to Antao (2013); Volume of X, Y and Z sites calculated using the IVTON software (Balic Zunic and Vickovic 1996); Δ(X-O) = (X2-O)-(X1-O) (Ungaretti et al. 1995); α: tetrahedral rotation along the $\frac{1}{2}$ axis (Born and Zemann 1964); TAV and OAV: tetrahedral and octahedral, respectively, angle variance (Robinson et al. 1971); S(Y) and S(Z) stand for shared edges of octahedra and tetrahedra, respectively; U(Y) and U(Z) stand for unshared edges of octahedra and tetrahedra, respectively; t_{SY} and t_{SZ}: the distance between shared edges of octahedra and tetrahedra, respectively; t_{UY} and t_{UZ}: the distance between unshared edges of octahedra and tetrahedra, respectively; X-Y and X-Z: interatomic distance between the X cation and Y, and Z cation, respectively; φ: Si-O-Y angle (Yang et al. 2009).

Table 7. Structural formulae in atoms per formula unit (apfu) of the studied samples, selected literature Ti-garnets and natural end-member garnets.

	X site	Y site	Z site	φ site	SIMS data
Cation distribution from this study:					
W6	(Ca _{2.88} Mg _{0.07} Na _{0.05})Σ=3.00	(Mg _{0.08} Mn _{0.02} Fe ³⁺ _{0.88} Ti ³⁺ _{0.17} Ti ⁴⁺ _{0.84} Zr _{0.01})Σ=2.00	(Si _{2.29} Ti _{0.08} Fe ³⁺ _{0.38} Fe ²⁺ _{0.11} Al _{0.10} [] _{0.04})Σ=3.00	O _{11.84} OH _{0.16}	OH _{0.17} F _{0.002} Li _{0.001}
W12	(Ca _{2.98} Mn _{0.01} Na _{0.01})Σ=3.00	(Mg _{0.13} Fe ³⁺ _{1.18} Al _{0.09} Ti ³⁺ _{0.06} Ti ⁴⁺ _{0.54})Σ=2.00	(Si _{2.58} Fe ³⁺ _{0.28} Al _{0.12} [] _{0.02})Σ=3.00	O _{11.92} OH _{0.08}	OH _{0.10} F _{0.003} Li _{0.001}
W16	(Ca _{2.88} Mg _{0.06} Na _{0.06})Σ=3.00	(Mg _{0.06} Mn _{0.02} Fe ³⁺ _{0.15} Fe ³⁺ _{0.73} Al _{0.10} Ti ³⁺ _{0.11} Ti ⁴⁺ _{0.81} Zr _{0.02})Σ=2.00	(Si _{2.38} Ti _{0.08} Fe ³⁺ _{0.50} Fe ²⁺ _{0.02} [] _{0.02})Σ=3.00	O _{11.92} OH _{0.07} F _{0.01}	OH _{0.12} F _{0.010} Li _{0.001}
NZALA	(Ca _{2.96} Mg _{0.02} Na _{0.02})Σ=3.00	(Mg _{0.07} Mn _{0.04} Fe ²⁺ _{0.12} Fe ³⁺ _{1.09} Cr _{0.01} Al _{0.05} Ti ⁴⁺ _{0.61} Zr _{0.01})Σ=2.00	(Si _{2.64} Fe ³⁺ _{0.29} Al _{0.06} Fe ²⁺ _{0.01})Σ=3.00	O _{12.00}	OH _{0.05} F _{0.005} Li _{0.003}
ZER2	(Ca _{2.97} Mg _{0.03} Li _{0.01})Σ=3.01	(Mg _{0.02} Mn _{0.01} Fe ³⁺ _{1.46} Cr _{0.01} Al _{0.18} Ti ³⁺ _{0.21} Ti ⁴⁺ _{0.10} Zr _{0.01})Σ=2.00	(Si _{2.88} Al _{0.07} [] _{0.05})Σ=3.00	O _{11.80} OH _{0.20}	OH _{0.25} F _{0.001} Li _{0.005}
Cation distribution after Grew et al. (2013):					
W6	(Ca _{2.88} Fe _{0.05} Mn _{0.02} Na _{0.05})Σ=3.00	(Mg _{0.15} Fe ²⁺ _{0.23} Fe ³⁺ _{0.52} Ti _{1.09} Zr _{0.01})Σ=2.00	(Si _{2.29} Fe ³⁺ _{0.57} Al _{0.10})Σ=2.96	O _{11.82} OH _{0.18}	
W12	(Ca _{2.98} Mn _{0.02} Na _{0.01})Σ=3.01	(Mg _{0.13} Fe ²⁺ _{0.06} Fe ³⁺ _{1.20} Ti _{0.60})Σ=1.99	(Si _{2.58} Fe ³⁺ _{0.18} Al _{0.21})Σ=2.97	O _{11.90} OH _{0.10}	
W16	(Ca _{2.87} Fe _{0.05} Mn _{0.02} Na _{0.06})Σ=3.00	(Mg _{0.12} Fe ²⁺ _{0.24} Fe ³⁺ _{0.62} Ti _{1.00} Zr _{0.02})Σ=2.00	(Si _{2.37} Fe ³⁺ _{0.49} Al _{0.10})Σ=2.96	O _{11.86} OH _{0.13} F _{0.01}	
NZALA	(Ca _{2.96} Mn _{0.02} Na _{0.02})Σ=3.00	(Mg _{0.10} Mn _{0.02} Fe ²⁺ _{0.12} Fe ³⁺ _{1.15} Cr _{0.01} Ti _{0.61} Zr _{0.01})Σ=2.02	(Si _{2.63} Fe ³⁺ _{0.24} Al _{0.12})Σ=2.99	O _{11.94} OH _{0.05} F _{0.01}	
ZER2	(Ca _{2.96} Fe _{0.02} Mn _{0.02})Σ=3.00	(Mg _{0.06} Fe ²⁺ _{0.19} Fe ³⁺ _{1.25} Al _{0.19} Cr _{0.01} Ti _{0.31} Zr _{0.01})Σ=2.02	(Si _{2.87} Al _{0.06} Li _{0.01})Σ=2.94	O _{11.74} OH _{0.26}	
Müntener and Hermann (1994)	Ca _{3.00}	(Fe ³⁺ _{1.24} Fe ²⁺ _{0.12} Mn _{0.01} Ca _{0.07} Cr _{0.02} Al _{0.06} Ti ⁴⁺ _{0.31} Ti ³⁺ _{0.17})Σ=2.00	(Si _{2.80} Al _{0.11} [] _{0.09})Σ=3.00	O _{11.64} OH _{0.36}	
Ulrych et al. (1994)	(Ca _{2.904} Mg _{0.015} Mn _{0.003} Fe ²⁺ _{0.024} Na _{0.011} K _{0.005})Σ=2.962	(Fe ³⁺ _{1.206} Mg _{0.082} Zr _{0.006} Al _{0.551} Ti _{0.155})Σ=2.000	(Si _{2.799} [] _{0.205})Σ=3.00	O _{11.181} OH _{0.792} F _{0.028}	
Katerinopoulou et al. (2009)	(Ca _{2.99} Mg _{0.03})Σ=3.02	(Fe ³⁺ _{0.67} Cr _{0.54} Al _{0.33} Ti _{0.29} Zr _{0.15})Σ=1.98	(Si _{2.42} Al _{0.14} Ti _{0.24} Fe ³⁺ _{0.18})Σ=2.98	O _{11.89} OH _{0.11}	
Antao (2013)	(Ca _{2.964} Mg _{0.010} Mn _{0.026})Σ=3.000 (Ca _{2.960} Mg _{0.012} Mn _{0.028})Σ=3.000	(Mg _{0.083} Fe ³⁺ _{1.608} Fe ²⁺ _{0.006} Cr _{0.001} Al _{0.007} Ti ⁴⁺ _{0.295})Σ=2.00 (Mg _{0.121} Fe ³⁺ _{1.401} Fe ²⁺ _{0.023} Ti ⁴⁺ _{0.455})Σ=2.00	(Si _{2.795} Al _{0.205})Σ=3.000 (Si _{2.689} Al _{0.200} Fe ³⁺ _{0.111})Σ=3.000	O _{12.000} O _{12.000}	
Adamo et al. (2011)	Ca _{3.000}	(Ti _{0.002} Al _{0.005} Cr _{0.017} Fe ³⁺ _{1.952} Mn _{0.001} Mg _{0.016})Σ=1.993	Si _{3.008}	O ₁₂	
Locock et al. (1995)	(Ca _{2.866} Mn _{0.019} Mg _{0.080} Na _{0.038})Σ=3.003	(Mg _{0.055} Mn _{0.013} Fe ²⁺ _{0.057} Fe ³⁺ _{0.631} V ³⁺ _{0.014} Al _{0.137} Ti ⁴⁺ _{1.058} Zr _{0.039})Σ=2.004	(Si _{2.348} Fe ³⁺ _{0.339} Fe ²⁺ _{0.311} [] _{0.005})Σ=3.003	O ₁₂	
Chakhmouradian and McCammon (2005)	(Ca _{2.899} Mn _{0.020} Fe ²⁺ _{0.058} Na _{0.023})Σ=3.000	(Mg _{0.156} Fe ²⁺ _{0.197} Fe ³⁺ _{0.556} Al _{0.049} Ti _{0.959} Zr _{0.080} Nb _{0.003})Σ=2.000	(Si _{2.302} Al _{0.171} Fe ³⁺ _{0.497} [] _{0.030})Σ=3.000	O _{11.880} OH _{0.120}	
Antao (2014)	(Ca _{2.91} Mg _{0.05} Mn ²⁺ _{0.03})Σ=2.99	(Ti _{1.09} Fe ³⁺ _{0.46} Fe ²⁺ _{0.37} Mg _{0.08})Σ=2.00	(Si _{2.36} Al _{0.14} Fe ³⁺ _{0.51})Σ=3.01	O ₁₂	
Novak and Gibbs (1971)	(Ca _{2.96} Mn _{0.04})Σ=3.00	(Al _{1.95} Fe _{0.05})Σ=2.00	Si _{3.00}	O ₁₂	
Schingaro et al. (2001)	(Ca _{2.97} Ba ²⁺ _{0.03})Σ=3.00	(Mg _{0.11} REE ³⁺ _{0.02} Zr ⁴⁺ _{1.12} Ti ⁴⁺ _{0.68} Fe ³⁺ _{0.07})Σ=2.00	(Si _{1.33} Al _{0.81} Fe ³⁺ _{0.85})Σ=2.99	O ₁₂	
Scordari et al. (1999)	(Ca _{2.75} Mg _{0.05} Mn ²⁺ _{0.07} Fe ²⁺ _{0.13})Σ=3.00	(Ti ⁴⁺ _{0.04} Ti ³⁺ _{0.12} Fe ³⁺ _{1.12} Fe ²⁺ _{0.05} Al _{0.67})Σ=2.00	(Si _{2.88} Ti _{0.05} Fe ³⁺ _{0.04})Σ=2.97	O _{11.83} OH _{0.17}	

Table 8. Comparison of refined bond distances (Å) and mean atomic numbers (electrons, e⁻) of cation sites as determined by structure refinement (X-ref) and EPMA for the studied crystals. Average error on mean atomic number ± 0.5 e⁻.

	W6	W12	W16	NZALA	ZER2
Y-O _{X-ref}	2.008(1)	2.008(1)	2.010(1)	2.0121(4)	2.009(1)
Y-O _{EPMA*}	2.014	2.015	2.018	2.022	2.017
Y-O _{EPMA**}	2.025	2.019	2.026	2.032	2.030
Z-O _{X-ref}	1.684(1)	1.671(1)	1.681(1)	1.6615(4)	1.656(1)
Z-O _{EPMA*}	1.696	1.669	1.687	1.666	1.648
Z-O _{EPMA**}	1.692	1.666	1.689	1.665	1.650
m.a.n.(X) _{X-ref}	20.00	20.00	20.00	20.00	20.00
m.a.n.(X) _{EPMA*}	19.66	19.99	19.66	19.89	19.93
m.a.n.(X) _{EPMA**}	19.98	20.07	19.95	19.97	20.07
m.a.n.(Y) _{X-ref}	22.50	22.52	22.46	23.31	23.10
m.a.n.(Y) _{EPMA*}	23.48	23.31	23.22	24.01	24.13
m.a.n.(Y) _{EPMA**}	22.84	23.76	23.30	24.39	24.05
m.a.n.(Z) _{X-ref}	15.85	14.75	15.74	14.61	14.00
m.a.n.(Z) _{EPMA*}	15.95	14.99	16.20	15.18	13.74
m.a.n.(Z) _{EPMA**}	16.06	14.51	15.74	14.87	13.66
<i>Note:</i> *according to our cation distribution; **according to the Grew et al. (2013) cation distribution.					